J. Fluid Mech. (1971), *vol.* 47, *part* 3, *pp.* 547–576
Printed in Great Britain

Stability of the flow in a differentially heated inclined box

By JOHN E. HART†
Department of Meteorology, M.I.T., Cambridge, Massachusetts

(Received 9 June 1970)

The effect of sloping boundaries on thermal convection is studied theoretically and in the laboratory in the context of a model in which fluid is contained in a differentially heated rectangular box of small aspect ratio (depth/length), inclined at an angle δ to the vertical. Like its two limiting cases, Bénard convection and convection in the vertical slot, a basic state which exists for low Rayleigh numbers becomes unstable as this parameter is increased. The types of instability and indeed the manner in which the motions become turbulent depend crucially on δ. In our work with water the following general picture of the primary instabilities applies:

(i) For $90° > \delta > 10°$ with the bottom plate hotter, the instabilities are stationary longitudinal convectively driven rolls with axes oriented up the slope. Near $\delta = 10°$ there is an upper and lower Rayleigh number cut off. If the Rayleigh number is too small diffusion damps the instabilities, but if it is too large they are damped by the development of a stable upslope temperature gradient in the mean flow.

(ii) For $10° > \delta > -10°$ (negative angles imply a hotter upper plate), transverse travelling waves oriented across the slope are the first instabilities of the mean flow. They obtain their kinetic energy via the working of the upslope buoyancy force.

(iii) For $-10° > \delta > -85°$ longitudinal modes are again observed. These are rather curious in that they may exist when the stratification $-\hat{g}.\nabla T$ is everywhere positive. The necessary energy for these modes comes out of the mean velocity field and out of the mean available potential energy.

Agreement between the stability theory and the experiments is generally quite good over the whole range of δ, considering the approximations involved in finding a suitable basic flow solution.

For Rayleigh numbers less than $\sim 10^6$ turbulence is only possible for positive angles. For $85° > \delta > 20°$ the development of unsteadiness involves the occurrence and the breaking of wavy longitudinal vortices in a manner reminiscent of the development of turbulence in cylindrical Couette flow.

---

† Present address: D.A.M.T.P., Cambridge University.

1. Introduction

This paper reports on a study of thermal convective flows between differentially heated sloping plates. The study was originally motivated by a desire to find out what effect slope would have on certain thermally driven flows which are found in the atmosphere or the ocean. The occurrence of slope heating problems is rather common since rarely is the earth's surface aligned with geopotential lines. The problem, as will be formulated shortly, is closely tied up with two others which form the classic examples of thermal convection, namely the flows between differentially heated horizontal or vertical plates. The horizontal parallel plate convection case is well known and includes recent studies of critical motions by Davis (1967), Segel (1969) and Koschmieder (1966). The vertical case has a non-trivial basic circulation which was given theoretical consideration by Batchelor (1954). The same problem has been treated more recently in terms of a boundary-layer analysis by Gill (1966). Experiments on the flows in the vertical slot have been reported by Eckert & Carlson (1961) and by Elder (1965*a*, *b*), among others. Flow instabilities exist in this system as both stationary and travelling disturbances. The stationary ones have been discussed by Gershuni (1953), Rudakov (1967) and Vest & Arpaci (1969) and the travelling ones by Rudakov and by Gill & Davey (1969). We mention these instabilities because it is important to determine to what extent the instabilities in the slant convective case resemble those occurring in either the horizontal or vertical limits. The inclined geometry introduces some rather profound phenomena which do not occur in either of these limits.

We consider the thermally driven flow between two perfectly conducting plates, separated by a distance D, and maintained at a temperature difference ΔT. In the laboratory it is not convenient to work with open ends since then the experiment is susceptible to rather poorly defined recirculation effects of the local environment. So instead of considering the 'infinite' plate problem we choose to look at the motions of a fluid contained in a shallow box inclined at an angle δ from the vertical. There has been some previous work on flows in this geometry. It seems that DeGraaf & Van der Held (1953) were the first to consider the tilted convection problem, and were probably the first to note that a small inclination away from 90° serves to break the plan-form degeneracy which exists for infinitesimal instabilities in a horizontal convecting layer. As they were concerned with measuring the heat flow across the gap they did not offer an explanation for the observed longitudinal (oriented upslope) instabilities. Kurtweg (1970) considers the stability problem between infinite inclined plates, and shows that this problem for the onset of the longitudinal modes is essentially that of Rayleigh (1916) with reduced gravity $g \sin \delta$. He does not prove that this orientation is indeed the most unstable nor why the transverse modes (oriented cross-slope) are stabilized. These questions were to some degree answered by Liang & Acrivos (1970), who did calculations for the flow in a slightly non-horizontal infinite channel with free boundaries. They were able to show that the longitudinal rolls were indeed the most unstable, and they likened the stabilizing of the transverse modes to similar damping which occurs when horizontal

convective instabilities are subject to a shear flow (Ingersoll 1966). There, the transverse perturbations feed energy into the mean velocity field. This comparison is not correct and it is shown in §6.1 that the transverse convective instabilities actually gain energy from the basic velocity field. Apparently the only authors who have considered the stability of transverse disturbances over the whole range of angles are Birikh *et al.* (1968) and Gershuni & Zhutkovitskii (1969). Their calculations are again for the infinite channel. In order to understand the laboratory flows for all δ one needs to consider non-zero aspect ratios (closed channels of finite length). The non-zero aspect ratio changes the mean flow significantly and makes the problem considerably more complicated and interesting. Some new types of instability are discovered which may be of considerable importance in more general stratified shear flows.

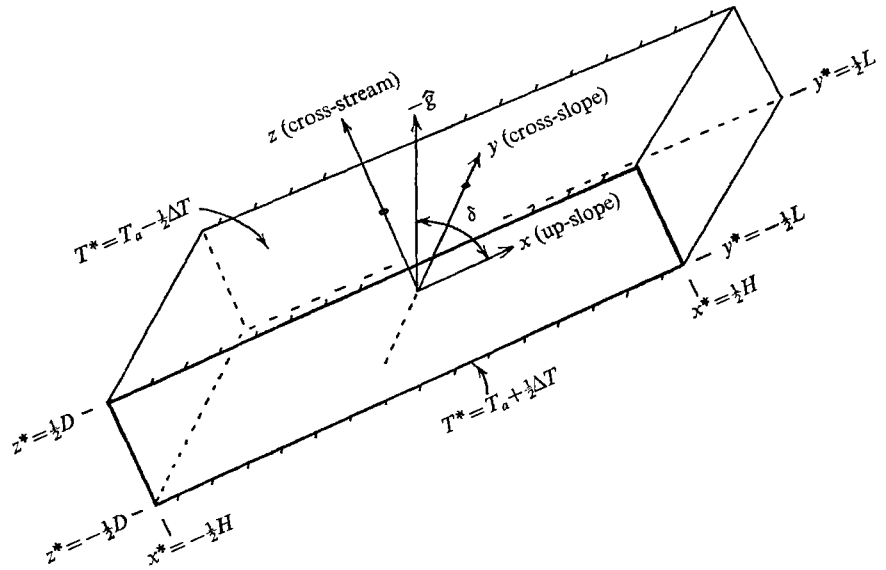

FIGURE 1. Co-ordinates and geometry for the problem.

To proceed formally we choose a local co-ordinate system rotated through δ with its origin at the centre of the box. The tank is constructed with rigid conducting boundaries at $z^* = \pm\frac{1}{2}D$, and with rigid insulating boundaries at $x^* = \pm\frac{1}{2}H$, $y^* = \pm\frac{1}{2}L$. The walls at $z^* = \pm\frac{1}{2}D$ are to be maintained at a temperature difference ΔT. The co-ordinate system and geometry are shown in figure 1. On the matter of notation the two possible kinds of heating can be achieved either by reversing the temperature difference, or by maintaining the direction of the heating, as in figure 1, and allowing δ to go to $-90°$. In the experiments δ was always positive and the plate temperature had to be reversed, but since the negative angle notation is more convenient in the presentation of the data we adapt it, noting: (i) if $90° \geqslant \delta > 0°$, the lower plate is hotter; (ii) if $0° > \delta \geqslant -90°$, the upper plate is hotter. Although we shall use negative angles to denote the second case, we stress again that the experiments and numerical calculations do not involve $\delta < 0°$, and statements like 'overhead view' should be interpreted accordingly.

The governing equations are taken to be the Navier–Stokes equations with the Boussinesq approximation. In non-dimensional form these are

$$G_r[\partial \mathbf{V}/\partial t) + \mathbf{V}.\nabla \mathbf{V}] = -\nabla p + \cos\delta T\hat{x} + \sin\delta T\hat{z} + \nabla^2 \mathbf{V}, \tag{1.1}$$

$$R_a[(\partial T/\partial t) + \mathbf{V}.\nabla T] = \nabla^2 T, \tag{1.2}$$

$$\nabla.\mathbf{V} = 0. \tag{1.3}$$

Here we have defined the Rayleigh number

$$R_a = g\gamma \Delta T D^3/\kappa\nu, \tag{1.4}$$

the Prandtl number $P_r = \nu/\kappa$,

and the numbers pertaining to the geometry, the tilt angle δ, and the aspect ratios D/L and D/H. We assume $D/L \to 0$ in this study so that only the one aspect ratio

$$h \equiv D/H \tag{1.5}$$

is important. The Grashof number $G_r = R_a/P_r$. In the above definitions ΔT is the magnitude of the applied temperature difference, $\mathbf{V}$ the velocity vector, T the temperature, g the gravitational acceleration, γ the coefficient of thermal expansion, ν the kinematic viscosity, and κ the thermal diffusivity. Velocities have the scale $g\gamma\Delta T D^2/\nu$, lengths D, temperature ΔT. The boundary conditions are that there be no normal flow nor any slip at any of the walls, that

$$T = \mp \tfrac{1}{2} \quad \text{at} \quad z = \pm \tfrac{1}{2}$$

and that $\nabla T.\hat{n} = 0$ at the other boundaries.

In the following sections we shall describe qualitatively what types of motion are observed in the experiment, and then go on to the theory for some of these motions. The theoretical results will then be compared to quantitative experimental data.

2. Description of the experiment

We have attempted to construct an experimental apparatus with appropriate velocity and temperature-measuring devices which is in direct correspondence to the idealized model. The tilt convection tank consists of two water-jackets each backing a precision ground, 1 cm thick, anodized aluminium plate. The two water-jackets are separated by a milled plexiglass spacer such that the region in between contains the working fluid. The dimensions of the working volume are $H = 38{\cdot}0$ cm, $L = 17{\cdot}8$ cm, and with two different spacers $D = 1{\cdot}521$ cm and $D = 1{\cdot}036$ cm. Micrometer measurements indicate that D is uniform to 0·005 cm. Two aspect ratios are available: $h = 0{\cdot}040$ and $h = 0{\cdot}027$.

Temperatures were measured by matched chromel–constantin thermocouples embedded in the plates or immersed in the working fluid. A stabilized nano-volt amplifier was used to drive a servo-potentiometer readout device. The system was calibrated to 0·01 °C, and fluctuations down to 0·002 °C could be measured. With this system it was determined that the plates could be maintained at temperatures constant within 0·005 °C or $0{\cdot}005\Delta T$, whichever was larger. The

thermal distribution across the plates was typically uniform to 0·01 °C or $0{\cdot}01\Delta T$, whichever was larger. Measurements in the fluid were for the most part accomplished through three variable micrometer-adjustable probes which traversed the z axis at $y = 0$; $x = 7{\cdot}45$ cm, 0 cm, $-7{\cdot}45$ cm. The thermocouples in these probes were 0·005 cm diameter, mounted as 1·2 cm cantilevers on 0·08 cm ceramic tubing. The probes were fed through the top plate.

Velocities were measured by photographing dye lines injected at strategic locations in the fluid. These were formed by stimulating a pH transition in a titrated solution of thymol blue indicator, a method which has been described by Baker (1966).

Of the parameters, R_a was measured within 2–6 %, with the higher limit for $R_a < 2000$. δ could be set within 0·12°. Unless otherwise noted the experiments were all done with water, $P_r = 6{\cdot}7$. The working fluid was outgassed and the thermocouple system calibrated before each run.

3. Qualitative observations of the various flow régimes

In order to get a general idea of the motions possible in this tilted geometry, we ran a series of experiments in which the top water-jacket was replaced with one which had a glass plate in place of the usual aluminium boundary surface. This enabled us to obtain a plan view of the circulations in the box by looking straight down through the upper bath. We took pictures, from this overhead view, of an aqueous suspension of ground fish-scales illuminated from the side by a collimated slit lamp. The first experiments were done with $\delta = 90°$ and with the bottom plate heated. In all these experiments where the Rayleigh number is slowly increased there is at first a primary state of motion followed by a series of secondary motions, then unsteadiness, and ultimately turbulence. The primary state for $\delta = 90°$ is known to be one of no motion, with a temperature distribution linear in z. Figure 2(a) (plate 1) shows the plan-form just above the well-known critical Rayleigh number, 1708. The secondary motion is in the form of rolls oriented parallel to the nearest side. The lateral boundaries apparently have an effect on the mode selection, as has been observed in a wider selection of geometries by Koschmieder. Davis (1967) has discussed the stability problem, including lateral walls, and the results agree qualitatively with our observations. Unsteadiness sets in around $R_a = 50000$, although a secondary striation structure appears on the rolls below this, near $R_a = 20000$. These effects have recently been discussed in more detail by Krishnamurti (1970).

At non-horizontal tilt angles the mode structure is rather different. There are no longer any transverse rolls, oriented parallel to the y axis. As the Rayleigh number is increased the first instabilities are completely longitudinal, oriented in the $\hat{x}$ direction. These modes are superimposed on a primary flow which has a non-zero velocity field. Because of the buoyancy component up the slope a single cell circulation is induced, with fluid flowing up the hot plate and down the cold one. Figure 3(a) (plate 2) shows how the primary instabilities develop for $\delta = 60°$ (the top boundary of the photograph is the most elevated end of the box). As the Rayleigh number is increased (figures 3(b)–(d), plate 2) one notices

the appearance of meanders on the longitudinal vortices. These grow to large amplitude as in figure 3(*c*) (plate 2), break, and eventually a state of violent unsteady mixing is reached (figure 3(*d*)). At this tilt angle, unsteadiness occurs at a Rayleigh number much lower than that required for violent unsteadiness in the horizontal convective case. The turbulence does not appear to be isotropic, the plumes being elongated in the x direction.

At $\delta = 20°$ the situation is somewhat similar. Longitudinal rolls are still the preferred mode of instability (figure 4(*a*), plate 3). At higher Rayleigh numbers there are intermittent periods of meanderings, but instead of leading to turbulence, steady states with higher wave-numbers ensue. This transition process is evident in figures 4(*b*), (*c*) (plate 3). Surprisingly, at this tilt angle the fluid cannot be driven to convective turbulence. As in figure 4(*d*) the rolls just disappear and the steady two-dimensional unicellular mean motion is all that remains at high $R_a (< 10^6)$.

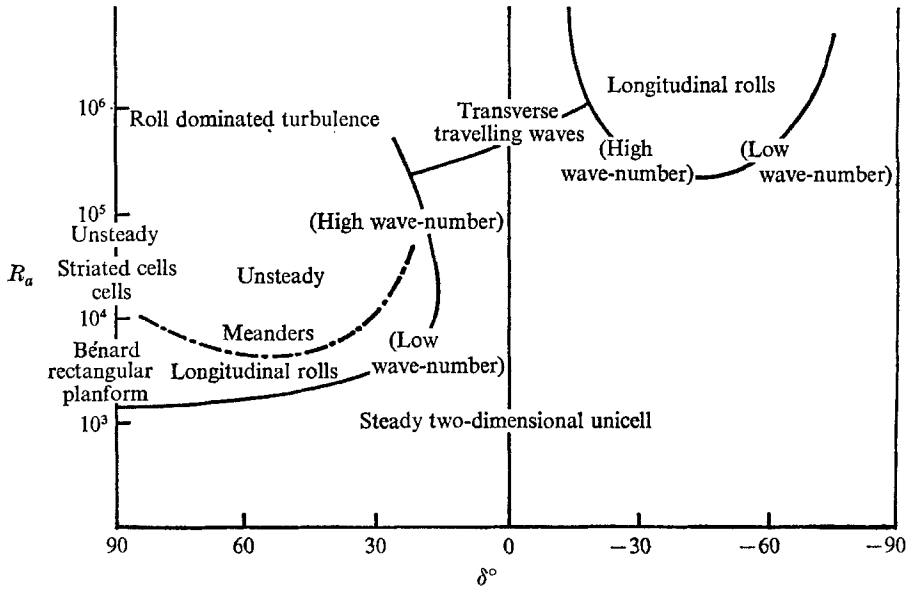

FIGURE 6. Sketch of régimes of motion.

Near $\delta = 0°$ the first instabilities are transverse travelling waves which are not easily visualized by this method. They are discussed in detail in §§7 and 8.

When the upper plate is hotter the flow at $R_a \lesssim 10^5$ is again a two-dimensional unicell. At sufficiently large R_a longitudinal instabilities are again observed. Figure 5 (plate 4) contains photographs of 3 cases, at different tilt angles. Instability occurs at very large negative angles, where one would intuitively expect the tank to be convectively stable.

From the information obtained from the visual study we have constructed a rough sketch of the types of motions in the tilt convection tank. Figure 6 contains this sketch. The centre-line is for $\delta = 0°$. To the left is the convectively unstable case. The left-hand boundary represents the familiar Bénard problem. The rough location of the transition points are included in the solid and dashed lines. The

remainder of this paper is an attempt to describe the events more quantitatively and to answer the questions that arise from the visual study. Some of this, it turns out, can be done theoretically. The preceding qualitative observations suggest that the more complicated régimes arise from instabilities of the unicellular flow. In the next three sections we consider a model of the basic circulation as determined from the velocity and temperature measurements, and the theoretical bounds on the stability of this model flow to different types of perturbations. The results of the linear stability theory are compared to more exact experimental results in § 8.

4. The primary circulation

4.1. *A parallel flow solution*

In this section we seek a mathematical description of the steady two-dimensional (x, z) basic flow in the sloping box. The equations governing this type of motion are obtained from (1.1)–(1.3) with $\partial/\partial t = \partial/\partial y = 0$. Then, denoting this basic flow with a subscript zero, we have

$$G_r(u_0 u_{0x} + w_0 u_{0z}) = -p_{0x} + \cos\delta T_0 + \nabla^2 u_0, \tag{4.1}$$

$$G_r(u_0 w_{0x} + w_0 w_{0z}) = -p_{0z} + \sin\delta T_0 + \nabla^2 w_0, \tag{4.2}$$

$$u_{0x} + w_{0z} = 0, \tag{4.3}$$

and

$$R_a(u_0 T_{0x} + w_0 T_{0z}) = \nabla^2 T_0. \tag{4.4}$$

There exists a parallel flow solution (where $u_0 = \bar{u}(z)$) of these equations. Under the assumption, to be discussed later, that the cross-stream buoyancy force $\sin\delta T_0$ is unimportant for the mean circulation we find that

$$T_0 = \beta x + \bar{T}(z) \tag{4.5}$$

and

$$u_0 = \bar{u}(z), \tag{4.6}$$

where

$$\bar{T} = -\frac{(\sin Mz\cosh Mz\tan\frac{1}{2}M/\tanh\frac{1}{2}M + \cos Mz\sinh Mz)}{2[(\tan\frac{1}{2}M\sin\frac{1}{2}M\cosh\frac{1}{2}M/\tanh\frac{1}{2}M + \cos\frac{1}{2}M\sinh\frac{1}{2}M)}, \tag{4.7}$$

and

$$\bar{u} = -\frac{\cos\delta}{4M^2}\frac{(\cos Mz\sinh Mz\tan\frac{1}{2}M/\tanh\frac{1}{2}M - \sin Mz\cosh Mz)}{(\tan\frac{1}{2}M\sin\frac{1}{2}M\cosh\frac{1}{2}M/\tanh\frac{1}{2}M + \cos\frac{1}{2}M\sinh\frac{1}{2}M)}. \tag{4.8}$$

This 'advective' solution depends on the parameter

$$M \equiv [\tfrac{1}{4}R_a\cos\delta\beta]^{\frac{1}{4}} \tag{4.9}$$

and on the arbitrary constant β.

Equations (4.5)–(4.9) represent an exact solution to the full non-linear governing equations for $\delta = 0°$, provided the conducting walls are maintained at $T_0 = \beta x \mp \frac{1}{2}$. The no-slip condition at $z = \pm\frac{1}{2}$ is satisfied. This solution was originally suggested by Elder (1965) and a discussion of its physical implications is contained there also. Vest & Arpaci (1969) and Gill & Kirkham (1970) have both used the above as a model base flow for studying the stability of fluid motion in the vertical slot. Of course the solution does not satisfy the isothermal wall boundary

conditions inherent in the experiments of Elder and Vest & Arpaci (and also our own), but the above authors extend the results from their stability calculations based on this solution to the experiments, under the tacit assumption that for small β it is a good approximation to what actually occurs near the centre of the apparatus. The experiments show that β is $O(h)$ (as we shall see in figure 8) so this assumption may be a good one for small aspect ratios. But in view of the well-known fact that stability equations of the Orr–Sommerfeld type can be quite sensitive to the shape of the mean profiles, we shall devote the next section to a detailed comparison of this parallel flow theory with our laboratory measurements of the mean circulation.

It should be noted that as M tends to zero, the mean fields described above tend to the 'conduction' solution which has

$$\bar{u} = (\cos\delta/6)\,(z^3 - \tfrac{1}{4}z) \tag{4.10}$$

and

$$T_0 = -z. \tag{4.11}$$

This is the exact solution for the buoyancy driven flow between infinite differentially heated isothermal plates. The stability of this flow has been studied recently by Birikh *et al.* (1968) and by Gershuni & Zhukovitskii (1969), and in principle these results can be applied directly to the experiments provided R_a and h are small enough that the conductive limit is accurate. Unfortunately the calculations published by these authors do not include $P_r = 6.7$.

4.2. *Comparison with the experiments*

We concentrate on the region $-0{\cdot}4 < xh < 0{\cdot}4$, since it is here that the instabilities are observed to develop. A dye line induced along $y = z = 0$ shows that $w_0 = 0$ except within regions of $O(D)$ from the ends. This observation, coupled with the velocity profile data, taken at the three thermocouple traverse points (§2), which show that u_0 is independent of x to within 5%, indicate that the parallel flow assumption is probably fairly good. The second assumption was that the cross-stream buoyancy is unimportant. From the y vorticity equation this means that

$$\cot\delta\, T_{0z}/T_{0x} \gg 1,$$

which can be anticipated on theoretical grounds provided $\cot\delta/h \gg 1$. The validity of this argument will be tested by seeing to what extent the measured profiles depend upon the reduced Rayleigh number, $R_a\cos\delta$, alone.

The theory predicts a constant upslope temperature gradient. Figure 7 shows some temperature traverses taken along $y = x = 0$. It is seen that over the region of interest the dependence is linear with x. The magnitude of the upslope gradient β is not given by the simple theory of the previous section, so we have determined it empirically by measuring the gradient at $x = y = z = 0$. The results are shown in figure 8. For tilt angles greater than $-70°$ the development of βh^{-1} occurs in a similar manner, rising from zero at $R_a\cos\delta \approx 1\times10^4$ to a value near 0·6 for $R_a\cos\delta > 5\times10^4$. This rise evidently marks the transition between the conductive and the advective behaviour of the mean flow. For $\delta < -70°$, βh^{-1} deviates from a pure dependence on the reduced Rayleigh number. That this

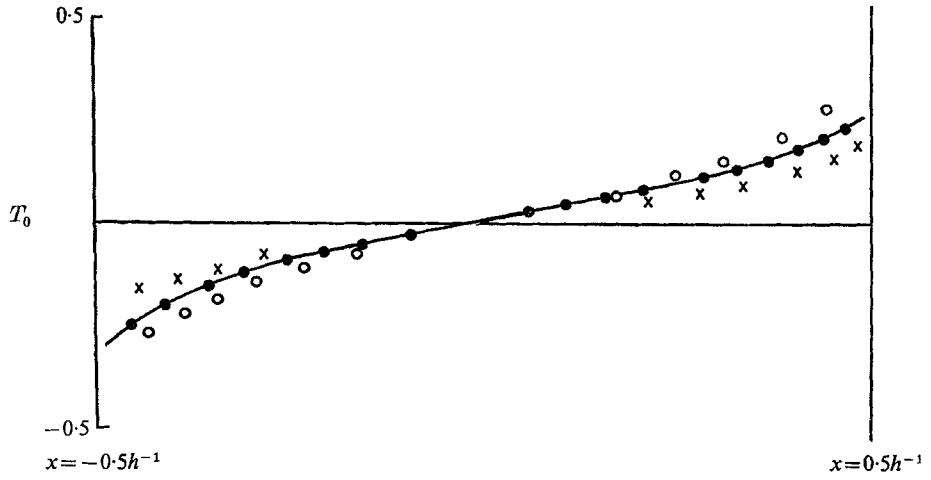

FIGURE 7. Upslope temperature distributions along $z = y = 0$.
$R_a = 5{\cdot}13 \times 10^4$, $P_r = 24$. ●, $\delta = 0°$; ×, $\delta = -60°$; ○, $\delta = -75°$.

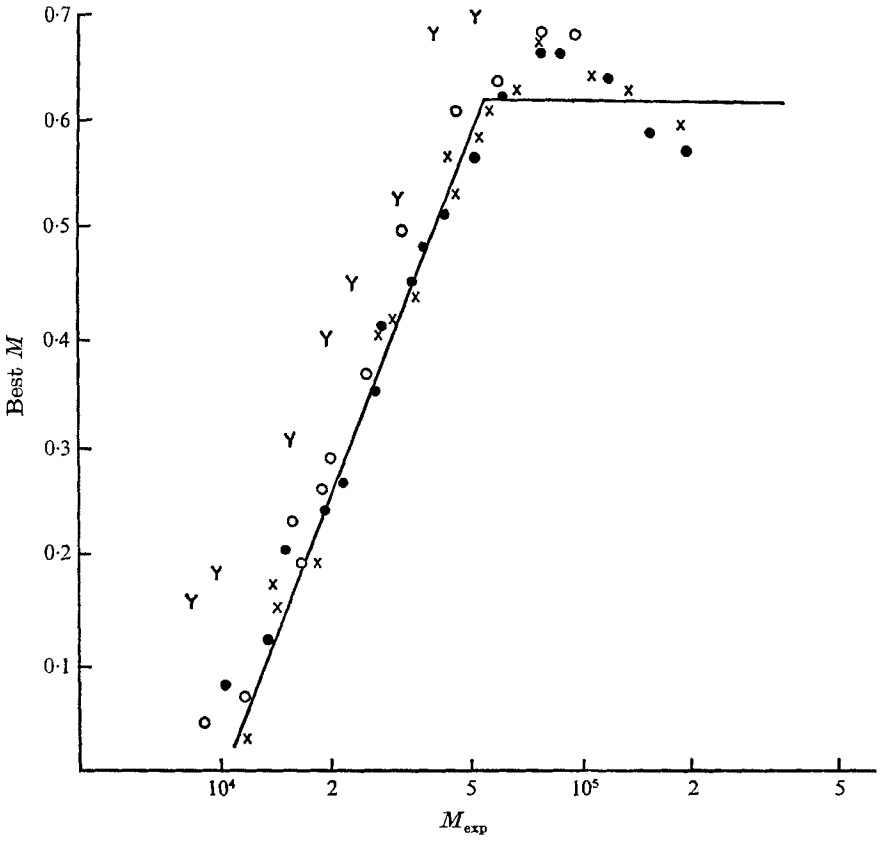

FIGURE 8. The upslope gradient of temperature at $x = z = y = 0$ as a function of the reduced Rayleigh number. ●, $\delta = 0°$; ×, $\delta = -30°$; ○, $\delta = -60°$; Y, $\delta = -75°$.

should happen is consistent with the breakdown of the assumed neglect of the cross-stream buoyancy force. At these almost horizontal angles $\cot\delta/h$ is no longer large with respect to one, and blocking in the corner regions becomes more efficient, with tongues of cool (warm) fluid penetrating into the central regions

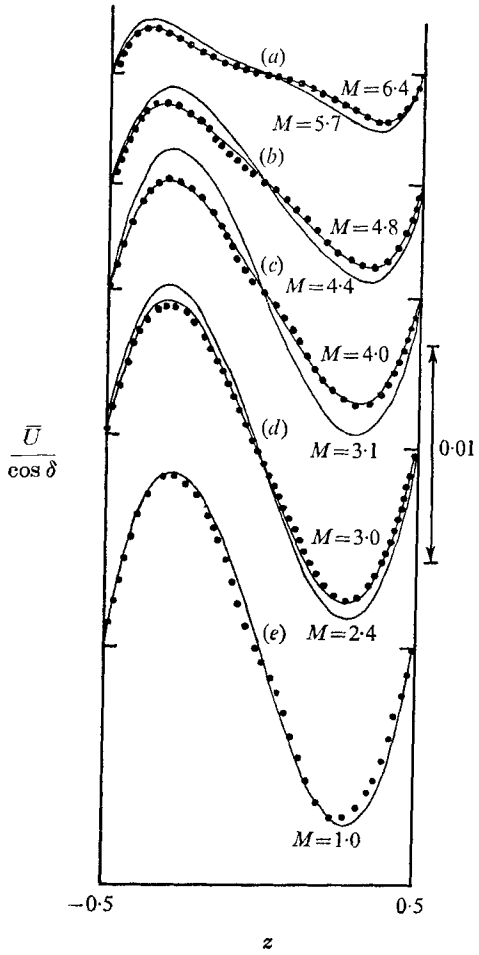

FIGURE 10. Some comparisons of typical velocity profiles with the theory (solid lines) calculated at the values of M shown. The points are for: (*a*) $M = 5{\cdot}7$, $\delta = 0°$; (*b*) $M = 4{\cdot}4$, $\delta = 0°$; (*c*) $M = 3{\cdot}1$, $\delta = -75°$; (*d*) $M = 2{\cdot}4$, $\delta = -60°$; (*e*) $M = 1{\cdot}0$, $\delta = 0°$.

from the lower (upper) corners. The blocking regions form because of the cross-stream buoyancy and are not expected to be the same for positive and negative angles. The theory for the mean flow in a slightly non-horizontal box (Hart 1971) shows that the blocking effect is only important for negatives angles. In terms of instabilities and turbulence the region $\delta < -70°$ is of lesser interest.

We now compare the theory with the profile measurements at $x = y = 0$. The data were obtained by taking temperature traverses and by making use of the dye wire technique. Figure 9 (plate 5) shows a typical dye trace in the region where the mean flow is 'advective'. Note the tendency towards a stagnant layer

near $z = 0$. The velocity data taken from photographs like this are believed to be accurate to better than 5 %. The values of β necessary for the theory were obtained from the solid line of figure 8. Typical comparisons are shown in figure 10. The velocity profiles fit the theory fairly well, but it was found that almost always the observed velocities were smaller than those in the theoretical profiles, except for small M, where the agreement is excellent (case *e*). As seen from the other four cases, the data do fit the predicted velocity distributions much better if these are calculated with an increased value of the parameter M.

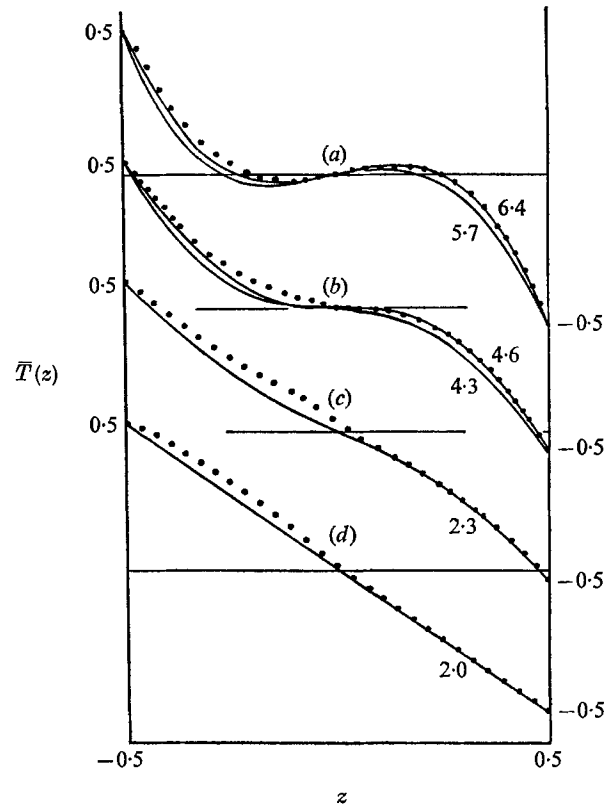

FIGURE 11. Some comparisons of observed temperature profiles with the theory (solid lines) calculated with the values of M shown. The points are the data for: (*a*) $M = 5{\cdot}7$, $\delta = 0°$; (*b*) $M = 4{\cdot}3$, $\delta = 0°$; (*c*) $M = 2{\cdot}3$, $\delta = -60°$; (*d*) $M = 2{\cdot}0$, $\delta = 0°$.

A similar situation seems to exist for the temperature distributions. Figure 11 shows some typical cases. As opposed to the velocity distributions the temperature profiles are not symmetric about $z = 0$. It is thought that this is due to the presence of the entry port which guides the probe into the working fluid through the wall at $z = -0{\cdot}5$. It is apparent that the variation of fluid properties with temperature does not play any role here, for if the temperature difference is reversed the non-symmetry still appears in the same sense as before. Since it is present for $\delta = 0°$ it could not be due to the neglect of the cross-stream buoyancy

either.† If we consider the temperature data for positive z, again we find that for experimental cases with small M the data agree with the theory but for larger values the best fit is obtained with a theoretical curve calculated with a slightly larger M.

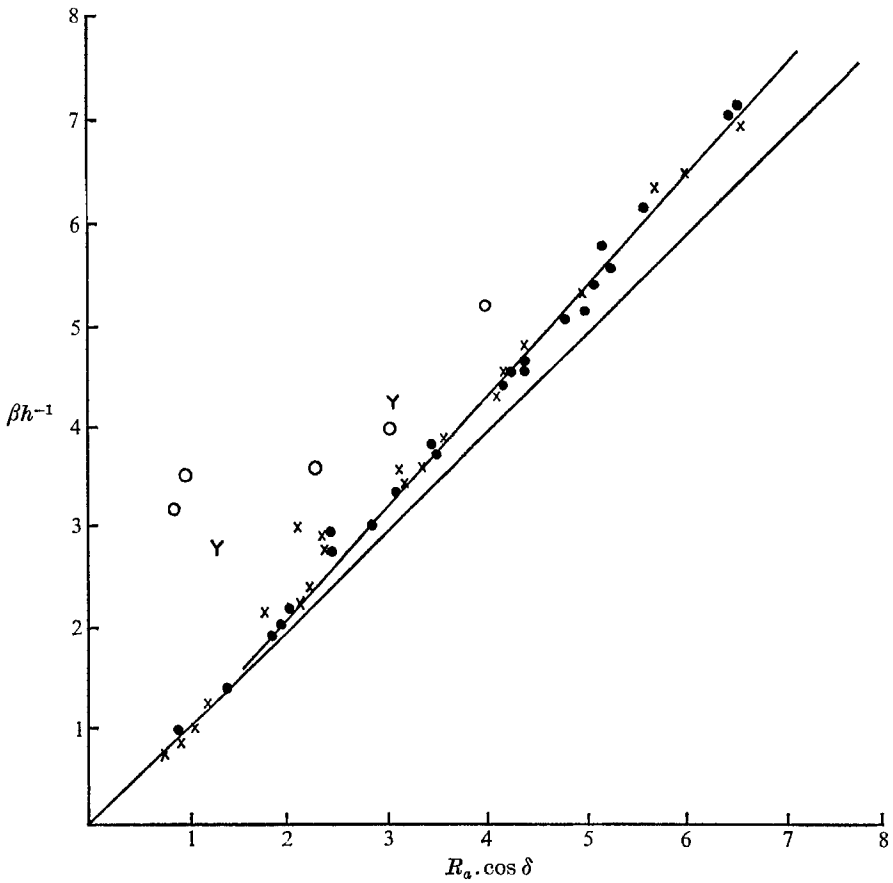

FIGURE 12. Summary of all the profile data. The plot shows the M which gives the best theoretical fit to the data, for each experimental case. ●, temperature, $\delta > -75°$; ×, velocity, $\delta > -75°$; ○, velocity, $\delta \leqslant -75°$; Y, temperature, $\delta \leqslant -75°$.

In figure 12 we summarize the comparison between the theory and all the velocity and temperature data. For $M_{\text{exp}} \gtrsim 2$ the data all fit the theoretical curves if M is related to M_{exp} by $M = 1{\cdot}09 M_{\text{exp}}$. The points at $\delta < -70°$ require rather higher M, consistent with the increase in the upslope temperature gradient observed at these high angles. That the theory consistently overestimates the observed fields when M_{exp} is large enough to be out of the conductive régime (e.g. $M > 2$) probably reflects the fact that the theory fails to reduce the upslope

† In fact the effect of this buoyancy term can easily be included in the solution (4.5)–(4.8). The main contribution is to add a small correction $\tan \delta \beta z$ to the mean temperature field, but this has the disadvantage of giving a multiparameter theory which is more difficult to fit to the data.

temperature gradient to zero on the walls. This overestimate by the theory shows up to a certain degree in Elder's (1965*a*) work also.

5. The linear stability problem

We wish to determine the values of R_a, h, P_r, and δ for which the mean fields specified by (4.5)–(4.9) become unstable to infinitesimal-amplitude perturbations. The mean fields are to be calculated with values of β which are empirically determined from the data (figure 8). We take

$$\beta = 0 \quad \text{for} \quad R_a \cos\delta < 10^4,$$

$$\beta = 0{\cdot}87(\log R_a \cos\delta - 4)h \quad \text{for} \quad 10^4 < R_a \cos\delta < 5{\cdot}2 \times 10^4,$$

$$\beta = 0{\cdot}62h \quad \text{for} \quad R_a \cos\delta > 5{\cdot}2 \times 10^4.$$

In view of the mean flow measurements we take $M = 1{\cdot}09(R_a \cos\delta\, \frac{1}{4}\beta)^{\frac{1}{4}}$. The governing equations (1·1)–(1·3) are linearized about $\bar{u}$ and T_0. We obtain, with primes denoting the perturbations,

$$G_r(u'_t + \bar{u}u'_x + w'\bar{u}_z) = -p'_x + \cos\delta\, T' + \nabla^2 u', \tag{5.1}$$

$$G_r(v'_t + \bar{u}v'_x) = -p'_y + \nabla^2 v', \tag{5.2}$$

$$G_r(w'_t + \bar{u}w'_x) = -p'_z + \sin\delta\, T' + \nabla^2 w', \tag{5.3}$$

$$R_a(T'_t + \bar{u}T'_x + w'\bar{T}_z + u'\beta) = \nabla^2 T', \tag{5.4}$$

$$u'_x + v'_y + w'_z = 0. \tag{5.5}$$

Since h and D/L are very small we can write all variables as

$$f' = \mathscr{R}\{f(z)\, e^{-i\omega t}\, e^{i(k_1 y + k_2 x)}\},$$

assuming that the perturbations will not be significantly affected by the sidewalls. There is no Squire's theorem for these perturbations. One can eliminate u, p and v from (5.1)–(5.3), obtaining, with $d = d/dz$ and $k^2 = k_1^2 + k_2^2$,

$$(d^2 - k^2)^2 w - iG_r[(k_2\bar{u} - \omega)(d^2 - k^2)w - k_2\bar{u}_{zz}w] - k^2 \sin T - ik_2 \cos\delta\, dT = 0. \tag{5.6}$$

The thermal equation is

$$(d^2 - k^2)T - iR_a[(k_2\bar{u} - \omega)T] - R_a w\bar{T}_z - R_a u\beta = 0. \tag{5.7}$$

The above two equations apply to arbitrary orientation, but we still need to specify $u(w, T)$. For $k_1 = 0$ (transverse waves)

$$u = i\, dw/k_2. \tag{5.8}$$

For $k_2 = 0$ (longitudinal rolls)

$$(d^2 - k^2)u + \cos\delta\, T - G_r w\bar{u}_z + iG_r\omega u = 0. \tag{5.9}$$

These are the only two cases in which the original set may be reasonably simplified. Fortunately these two 'simplest' cases describe just those modes which we observe, and we will leave the discussion of oblique modes for another time. For the simple conductive profile Gershuni & Zhukovitskii have shown that the oblique modes are never the most unstable.

We must solve the appropriate sets of equations subject to boundary conditions at the walls. For the experimental situation these are rigid and highly conductive.

We must have

$$u = w = dw = T = 0 \quad \text{at} \quad z = \pm\tfrac{1}{2}.$$

The kinetic energy balance for the perturbations is

$$(\partial/\partial t)\tfrac{1}{2}\langle u'^2+v'^2+w'^2\rangle = \cos\delta\langle u'T'\rangle+\sin\delta\langle w'T'\rangle - G_r\langle u'w'\bar{u}_z\rangle-\langle\nabla u'^2+\nabla v'^2+\nabla w'^2\rangle,$$

with brackets defining the average in z and over one spatial cycle.

The numerical solution is based on the Galerkin method (Mikhlin 1964 is a comprehensive reference). The variables are written in N-term expansions of complete orthogonal trial functions satisfying the appropriate boundary conditions. The methods and trial functions we have used are essentially those of Gallagher & McD. Mercer (1965). For the transverse modes, governed by (5.6)–(5.8), we obtain a $2N \times 2N$ real matrix eigenvalue problem. For longitudinal modes (5.6), (5.7) and (5.9) lead to a $3N \times 3N$ problem. The accuracy of the eigenvalue ω is tested by increasing N and requiring that: (i) $|\omega_{N+1}-\omega_N| \to 0$; (ii) the coefficients of the eigenfunctions converge in the above sense; (iii) the energy distribution balances. In some cases the computation can be considerably shortened by assuming $\omega = 0$, and finding $R_a(\delta, P_r, h, k)$ such that the residual determinant of the matrix is zero.

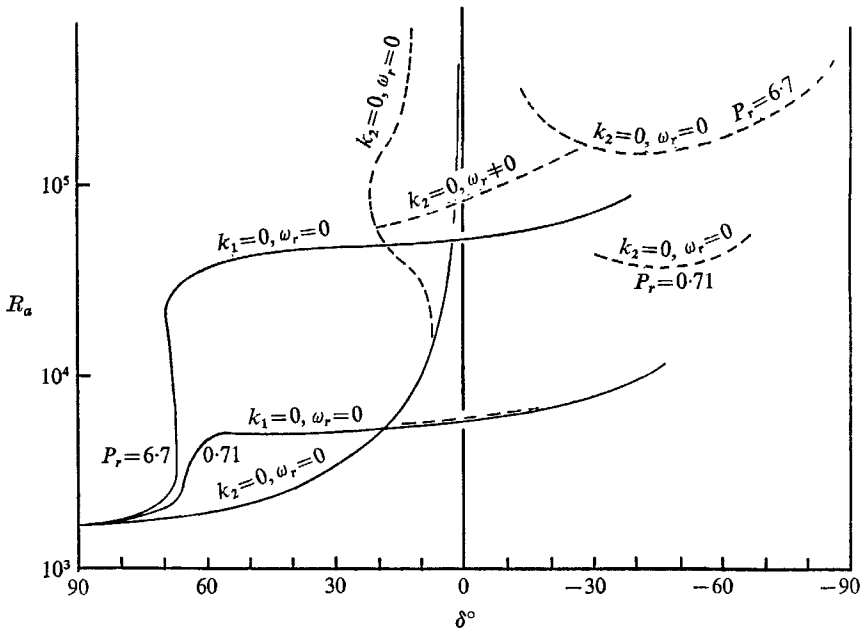

FIGURE 13. Critical Rayleigh numbers for the onset of infinitesimal disturbances. The solid lines are for the conductive limit, the dashed line has $h = 0{\cdot}04$.

Figure 13 contains the critical (neutral) curves for Rayleigh number as a function of δ. The solid line is for $h = 0{\cdot}0001$, which effectively means that the base flow corresponds to the conductive solution for all R_a. The dashed curve is for $h = 0{\cdot}04$. It is seen that almost all of the lowest or most unstable modes are

stationary. The only travelling disturbances are for the larger aspect ratio, the larger Prandtl number, and exist only near $\delta = 0°$. Away from this region the longitudinal instabilities ($k_2 = 0$) are the most unstable. The remaining stationary transverse modes fall basically into two categories. Near $\delta = 90°$ they are convective, the perturbations deriving most of their energy from the unstable temperature field. However, for $\delta < 60°$ the energy comes primarily out of the mean shear in the centre of the channel. The curves for $h = 0$, $k_1 = 0$, $\omega_r = 0$ are similar to those of Birikh *et al.* (1968), who did calculations for $P_r = 1$ and 5.

6. Discussion of the theoretical results

There is merit in giving some theoretical interpretation of the instabilities since the mean flow used is an exact solution to the full Navier–Stokes equations, under conditions specified in §4.1. If, for example, we did not use experimental data to connect β to R_a and δ, we would have a purely theoretical problem with an extra parameter. This sort of approach has been taken recently by Birikh *et al.* (1969), for $\delta = 0$. In our study we treat β as a dependent variable and confine our attention to the most unstable mode.

6.1. *Stationary transverse convective modes*

We begin by discussing the behaviour of the solutions in the convective region $90° \geqslant \delta \gtrsim 60°$. A value of $N = 12$ was sufficient to ensure numerical accuracy in the critical values of 1 %, along with energy convergence of the same order. We have solved the complete eigenvalue problem for certain test cases in this region to show that in fact the most unstable mode has $\omega_r = 0$. In figure 13 it is seen that the longitudinal modes are the most unstable in this region. The reasons for this behaviour become apparent when we consider the kinetic energy balance for these modes. Table 1 contains the results. We have defined e_ν = dissipation, e_u = upslope conversion = $\cos\delta\langle u'T'\rangle$, e_c = cross-stream conversion = $\sin\delta\langle\omega'T'\rangle$, e_I = transfer = $-\langle u'w'\overline{u}_z\rangle G_r$.

The longitudinal modes all have the same energy distribution as the $\delta = 90°$ case. The only kinetic energy generation for them is through the action of the cross-stream buoyancy force. At $\delta = 78°$ and $\delta = 66°$, $P_r = 6{\cdot}7$, it is seen that some small part of the kinetic energy of the transverse modes is actually supplied from the mean shear. This is in marked contrast to solutions of Ingersoll (1966) and others on convective instabilities in a plane horizontal Couette flow. There, transverse modes were stabilized by the mean motion. In our case the working against the upslope buoyancy is the effective stabilizing agent. The mechanisms by which these energy transformations come about are seen quite simply if we look at the eigenfunctions.

Figure 14 shows the isothermals and the stream function for $\delta = 78°$. At horizontal tilt the updrafts are vertical and are associated directly with the maxima of the temperature field. When the walls slope the updrafts still try to flow vertically, in the direction of the total buoyancy force. Relative to the boundaries this means that the streamlines must tilt into the mean shear. This is seen in figure 14, where the mean velocity field is up ($\hat{x}$) the bottom plate and

down the top. Thus the natural tendency of the flow to be in the direction of gravity causes the cell to take energy out of the mean velocity field. The damping is brought about by the phase shift in the thermal field; for example, when a hot plume, in order to complete a cell, must move downwards against the slope. Since the degree of shear interaction is roughly inversely proportional to the Prandtl number, cases with $P_r = 0{\cdot}71$ should be more unstable than say $P_r = 6{\cdot}7$. In the calculations of Gershuni & Zhukovitskii this effect is magnified to the point that transverse modes are the most unstable for $P_r = 0{\cdot}2$.

R_a	δ	P_r	h	e_v	e_u	e_c	e_I
1708	90°	6·7	0·0001	−1·000	0·0	1·000	0·0
1849	78°	6·7	0·0001	−1·000	−0·0239	1·0239	0·0005
3350	66°	6·7	0·0001	−1·000	−0·2241	1·2222	0·0018
1824	78°	0·71	0·0001	−1·000	−0·016	1·003	0·013
2697	66°	0·71	0·0001	−1·000	−0·107	0·986	0·119

TABLE 1. Energy balance for the stationary transverse convective modes

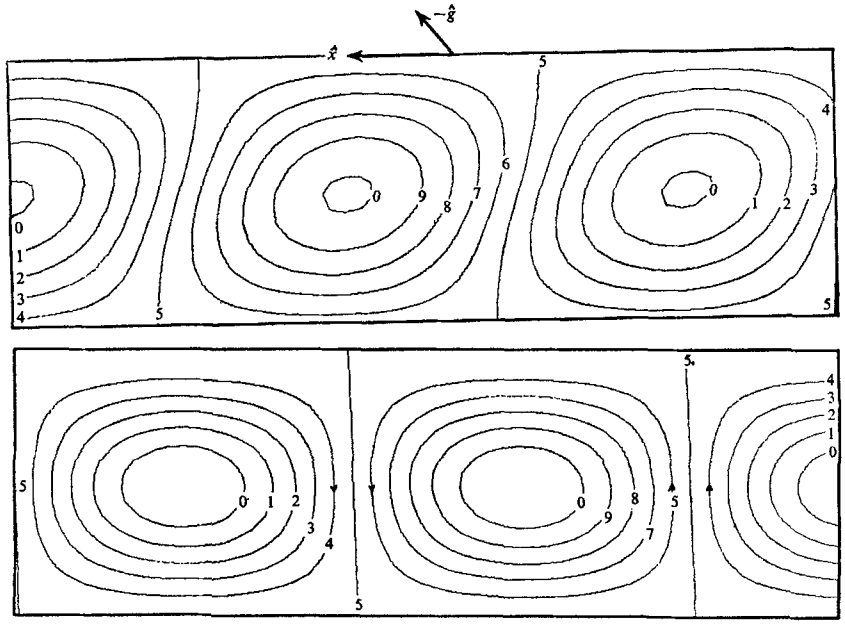

FIGURE 14. Contours of stream function (upper) and temperature (lower) with $P_r = 6{\cdot}7$, $h = 0{\cdot}0001$, $\delta = 78°$, $R_a = 1849$.

6.2. *Stationary transverse shear modes*

In this section we discuss the behaviour of modes with $\omega = k_1 = 0$ which exist for δ less than about 60°. These are shear instabilities, getting most of their energy from the mean velocity field. The neutral curves (calculated with $N = 12$) are shown in figure 13 for $h = 0{\cdot}0001$. The associated wave-numbers are 2·79 almost independent of δ. From table 2 it is seen that for $P_r = 6{\cdot}7$, $h = 0{\cdot}0001$, some

80 % of the kinetic energy of the perturbations come out of the mean shear. For $P_r = 0{\cdot}71$ this figure is of order 90 %.

For $\delta = 0°$ Vest & Arpaci (1969) find that there is no ($< 0{\cdot}5$ %) dependence of the critical curves on Prandtl number of P_r from zero to 10^3. Their method was essentially the same as the present one except they used smaller expansions with $N = 3$. We have found a slight dependence on P_r which is consistent with the energy calculations which indicate a sizeable contribution from e_u and e_c.

G_r	δ	P_r	h	e_v	e_u	e_c	e_I
7860	0°	6·7	0·0001	−1·000	0·199	0·0	0·790
8027	0°	0·71	0·0001	−1·000	0·060	0·0	0·927
7558	22°	0·71	0·0001	−1·000	0·022	0·103	0·874

TABLE 2. Energy balance for the stationary shear driven modes

R_a	δ	P_r	h	e_v	e_u	e_c	e_I
88900	0°	6·7	0·04	−1·000	1·130	0·0	−0·123
61900	17°	6·7	0·04	−1·000	0·995	0·118	−0·108
113000	−18°	6·7	0·04	−1·000	1·175	−0·052	−0·127

TABLE 3. Energy balance for the transverse travelling modes

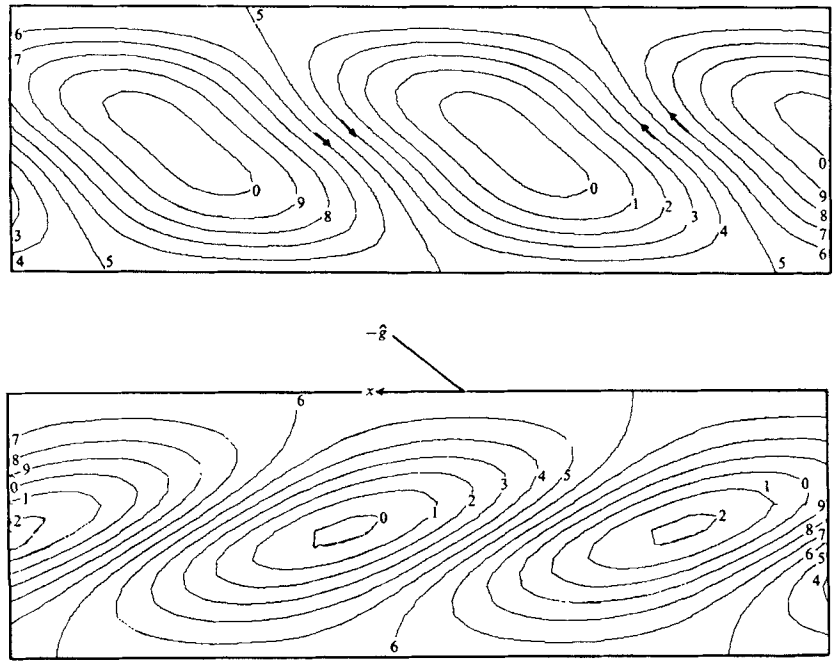

FIGURE 15. Contours of stream function (upper) and temperature for the transverse stationary mode with $P_r = 0{\cdot}71$, $h = 0{\cdot}0001$, and $\delta = 22°$.

Figure 15 shows contours of perturbation stream function and isotherms for one case. The instability is centred about the plane $z = 0$. The energy transfer is primarily from the shear at the centre of the slot.

When we make calculations for $h = 0{\cdot}027$ (thereby entering the advective base flow régime) we find that for $P_r = 0{\cdot}71$ the eigenvalues are nearly the same as before. At $P_r = 6{\cdot}7$, $h = 0{\cdot}027$ no solutions were found. Similar behaviour was noted by Vest & Arpaci, who stated that this absence of solutions was probably numerical.† The situation actually has a real physical basis which is not apparent in their remarks about the numerics. Figure 16 shows what happens as we take successively larger (but still small) values of h, at $\delta = 0°$. The critical curves form

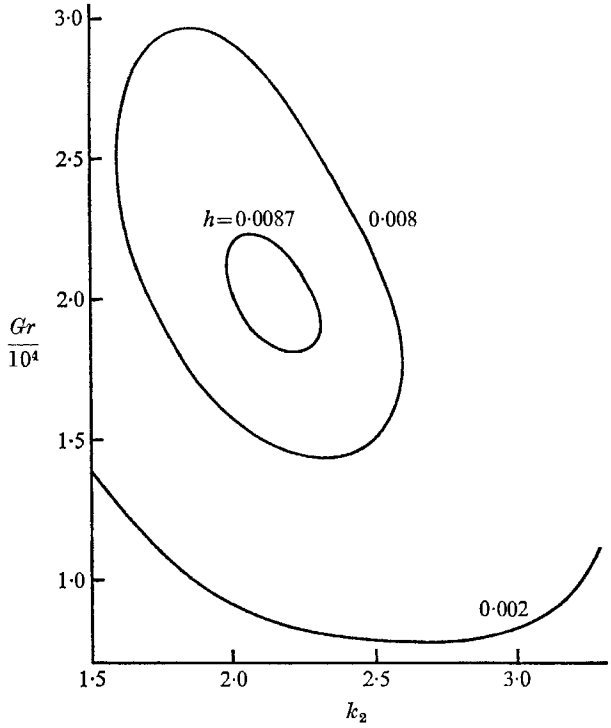

FIGURE 16. Neutral curves ($R_a(k_2)$) for stationary transverse modes as a function of h, with $P_r = 6{\cdot}7$.

closed loops with smaller internal areas as h becomes larger. Linear instabilities are only possible inside these loops and it is clear that instabilities can only exist for a finite range of G_r above onset. Indeed above $h = 0{\cdot}009$ or so these stationary modes just do not exist. This behaviour comes about physically because the mean profiles depend non-linearly on P_r and h. For these shear modes the critical parameter is G_r, and since they are centred and stationary, instability occurs when the Reynolds number near $z = 0$ is large enough. The profiles develop according to the value of $G_r P_r h$. But if this is large $(\partial u_0/\partial z)|_{z\sim 0}$ tends to zero. Therefore as G_r is raised instability will only be possible at large P_r if h is small enough. Of

† Vest & Arpaci only looked at the case with $\delta = \omega_i = \omega_r = 0$ and they erroneously neglected the last term of equation (5.7).

course these are rather crude physical arguments which naturally cannot include all that is described by the instability equations themselves, but the predictions are consistent with the numerical solutions.

6.3. *Transverse travelling modes*

The absence of growing stationary transverse disturbances at a Prandtl number of 6·7, for $h = 0{\cdot}04$, suggested that we look for travelling modes. These calculations were done with $N = 14$. The eigenvalues are believed to be accurate to 2 % or so. Some of the results are in figure 13 and others, including critical wavenumbers and frequencies, in §8. We note that the critical Rayleigh number increases as the tank becomes more convectively stable ($\delta \to -90°$). For the values of P_r and h used here the phase speeds are slightly lower than the maximum velocities of the mean profiles.

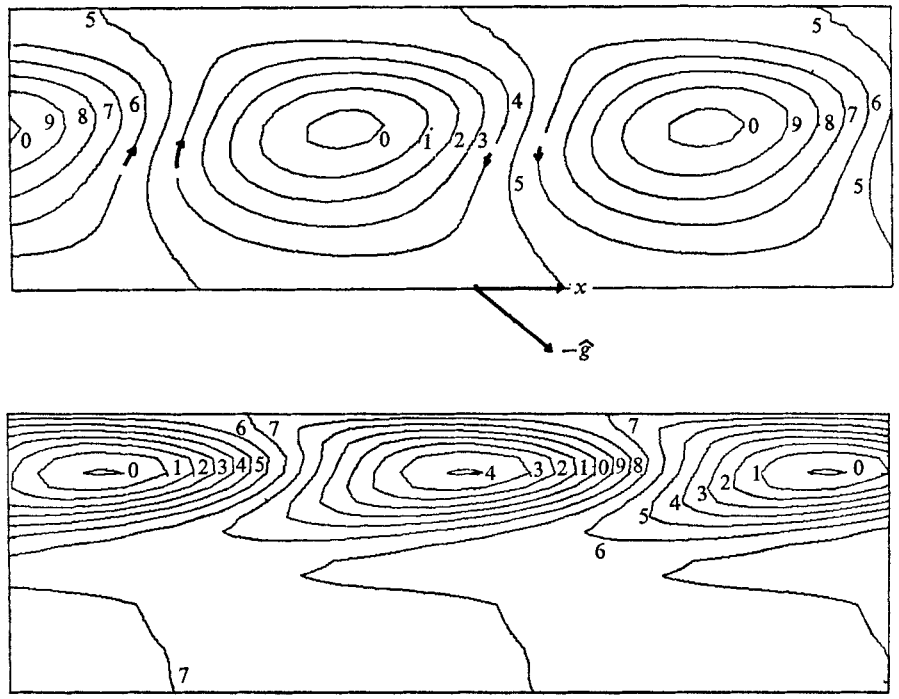

FIGURE 17. Contours of stream function and temperature for $\delta = 17°$, $P_r = 6{\cdot}7$ and $h = 0{\cdot}04$.

These modes cannot be called shear instabilities because they attain most of their kinetic energy via the conversion of upstream potential energy (see table 3). Because of the energy balance it is reasonable to suppose that these disturbances will be affected significantly by changes in the Prandtl number or in the tilt angle. The critical curves show that these modes are significantly more affected by these parameters than are the stationary modes of the previous section. Gill & Davey (1969) have discussed this type of buoyancy mode, which occurs in the

flow up a single heated vertical wall in a stratified fluid. This flow is approximately what one gets along one wall in the vertical slot provided $R_a h$ is large enough. They also find modes which are dominated energetically by e_u. The authors have tried to apply their results to the slot problem. For $P_r = 6{\cdot}7$, $h = 0{\cdot}04$ their critical Rayleigh number is approximately $R_a = 1{\cdot}07 \times 10^3$. This is considerably lower than the available experimental results, including those in the present study. It is clear that the boundary-layer flow model is not applicable at the values of R_a, P_r, and h, at which the instabilities are observed. Contours for our 'two-wall' solution are shown in figure 17. Although the isotherms are concentrated along the wall, the stream pattern reaches clear across the gap. The added damping caused by the stress on the opposite wall and by the effect of the reverse flow probably is why our critical Rayleigh number at $\delta = 0$ of $R_a = 8{\cdot}89 \times 10^4$ is considerably higher than Gill & Davey's.

6.4. *Longitudinal modes*

In this section we discuss modes which have $k_2 = 0$ and hence are oriented parallel to the $\hat{x}$ axis. We concentrated our calculations on the case $\omega_r = 0$ (although full calculations do indicate that this is indeed true for the most unstable modes). The calculation were done on the M.I.T.–I.B.M. 360 computer, which led to an upper limit of $N = 5$, and accuracy in the critical values estimated at 3 %.

The longitudinal modes are interesting in that there are many different stabilizing and destabilizing mechanisms inherent in the equations, all of which may influence the onset points for a specific set (P_r, h, δ). So before presenting the results which involve the complicated base flows and rigid boundaries, we present a brief discussion of these mechanisms. The equations for the neutral stability of the longitudinal modes are obtained from (5.6), (5.7), (5.9) by setting $k_2 = \omega_r = 0$. We find

$$(d^2 - k^2)^2 w - k^2 \sin \delta T = 0, \tag{6.1}$$

$$(d^2 - k^2) T - R_a w \bar{T}_z - R_a \beta u = 0, \tag{6.2}$$

$$(d^2 - k^2) u + \cos \delta T - G_r w \bar{u}_z = 0. \tag{6.3}$$

The only source of energy for the rolls (w, v part of the instability) is the conversion from cross-stream potential energy. To have these longitudinal modes one must have

$$\sin \delta \int_{-\frac{1}{2}}^{\frac{1}{2}} wT \, dz > 0, \tag{6.4}$$

a fact which may be obscured if the total kinetic energy balance is written down. The energy sources for cross-stream and upslope motions are rather different, but since the dynamics are coupled there are many feedback mechanisms which can satisfy (6.4). These mechanisms exist primarily because the temperature field can be generated by advection from either the complicated cross-stream gradient $\bar{T}_z$ or from the constant upslope gradient β.

Consider an updraft with $w > 0$, generated by a positive temperature perturbation $T > 0$. This will tend to generate vorticity. How can the motion sustain itself? In the usual Rayleigh convection problem the positive perturbation is regenerated by advection of temperature from the unstable mean field with

$\overline{T}_z < 0$ somewhere. If $\overline{T}_z > 0$ everywhere no such regeneration can occur and the motion is stable. In the present problem, however, the positive perturbation in $\overline{T}$ can also be reinforced by advection from the mean upslope thermal field βx. Here β is positive and feedback will occur only if u is negative. If the parameters are right, shear generated upslope velocity can cause longitudinal convective instabilities, even if the cross-stream temperature field is completely stable. The longitudinal vorticity is still driven convectively, but it is the mean shear

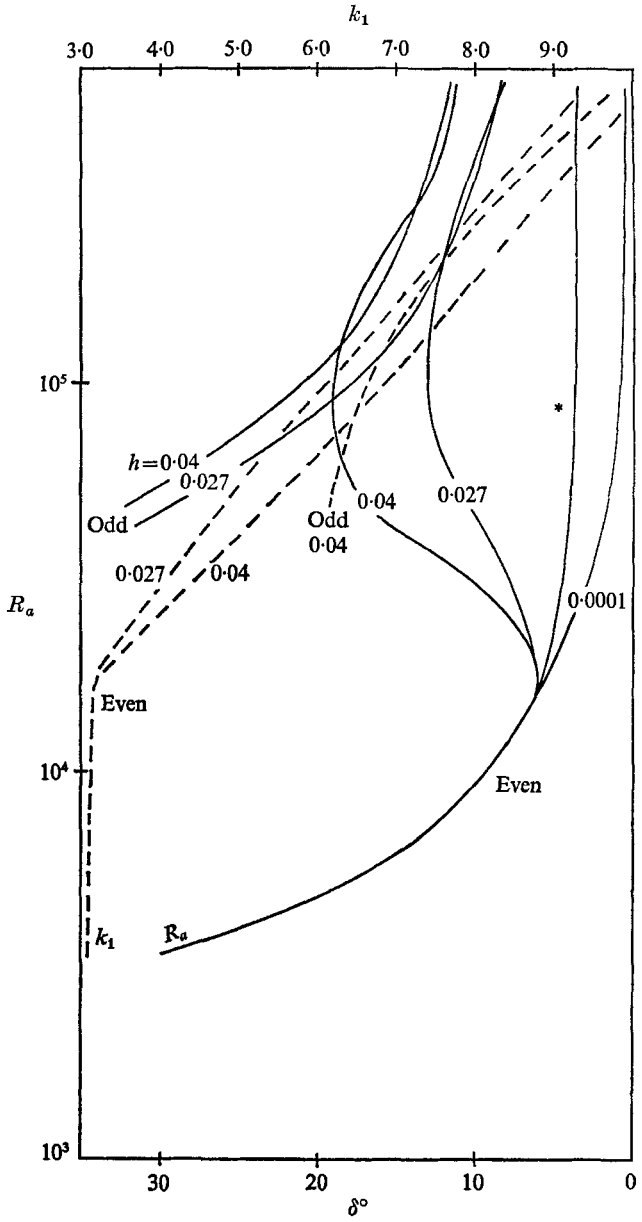

FIGURE 18. Neutral curves R_a (solid) and k_1 (dashed) with $\delta > 0°$, $P_r = 6{\cdot}7$, for the most unstable even and odd modes.

generated part of the total kinetic energy which allows regeneration. Naturally with our mean fields the solutions will contain all the above effects in complicated ways.

Figure 18 shows the results for $P_r = 6{\cdot}7$, $\delta > 0°$. The solid curves are the critical Rayleigh numbers. The $h = 0{\cdot}0001$ curve is just Kurtweg's simple solution $R_a = 1708/\sin\delta$. The curve labelled * is the purely convective problem based on $\bar{T}(z)$.† This case is just slightly more stable than the pure conductive-profile limit and just reflects the growth of a stable layer in T as M becomes large. Both these cases are quite different from the solutions for the complete problem,

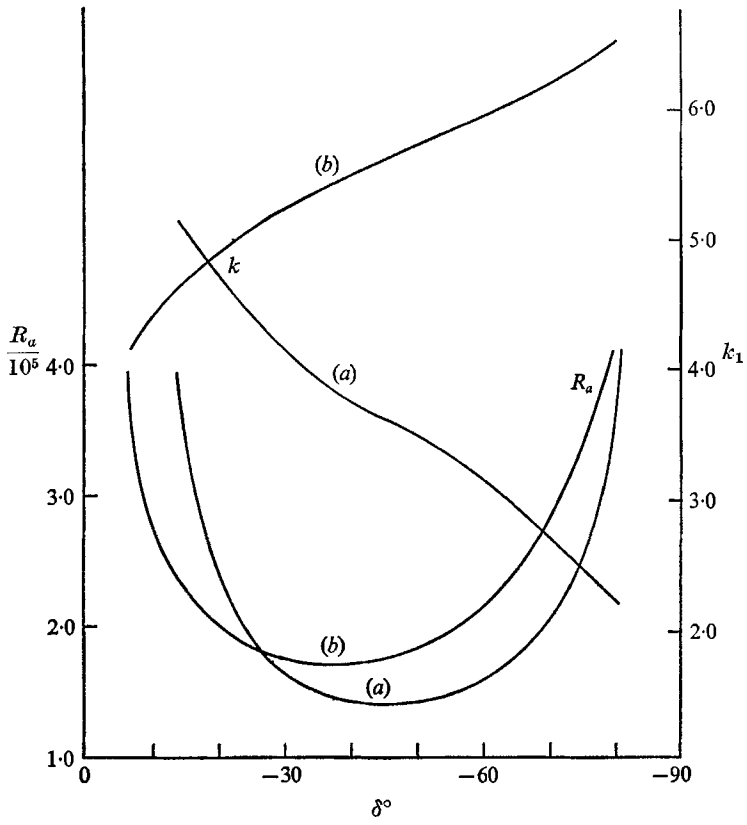

FIGURE 19. Neutral curves for R_a and k_1 calculated for $\delta > 0°$, $P_r = 6{\cdot}7$. See text for explanation of cases (*a*) and (*b*).

shown for $h = 0{\cdot}027$ and $h = 0{\cdot}04$. Energy must be put into the mean upslope (stable) temperature stratification. The wave-numbers increase with Rayleigh number as more efficient release of cross-stream potential energy is needed to feed this transformation.

Figure 19 shows the stability curves for $P_r = 6{\cdot}7$, $h = 0{\cdot}04$, with $\delta < 0°$. Curve (*b*) is again the purely convective problem.† Curve (*a*) is the complete solution.

† For this we have arbitrarily set $\beta = 0$ in equation (6.3). This decouples the instabilities from the mean velocity field.

The critical Rayleigh numbers behave in a similar way but the wave-number curves are entirely different. For case (*b*) instability is possible as a negative temperature gradient develops in $\overline{T}_z$. This is necessarily a small fraction of the gap so one would expect the associated wave-numbers to be large as they are. For the complete problem the wave-numbers decrease markedly as δ decreases.

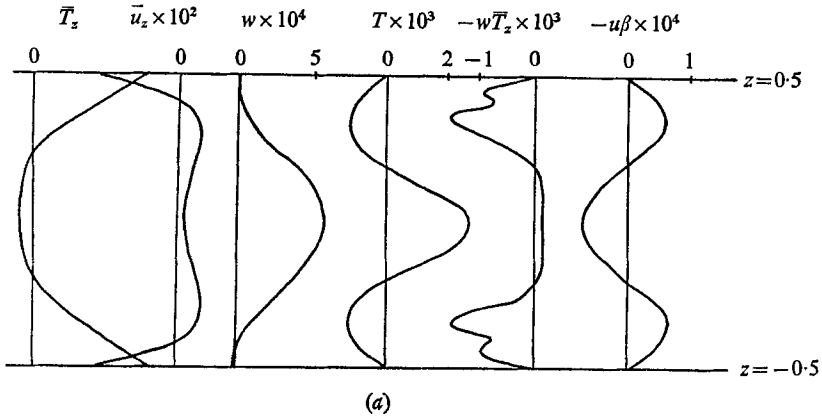

(*a*)

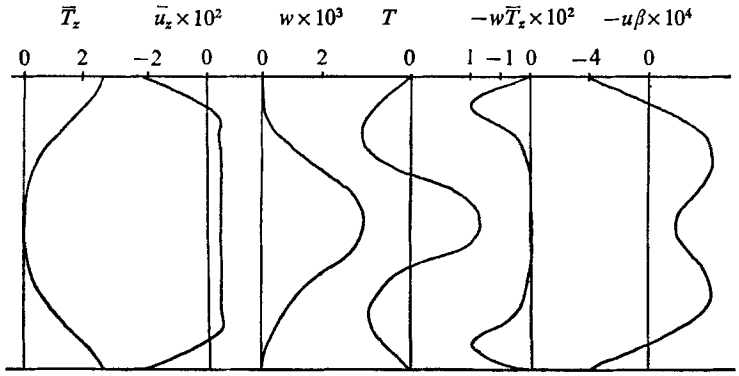

(*b*)

FIGURE 20. Solutions for $P_r = 6{\cdot}7$, $h = 0{\cdot}04$, with $\delta = -17°$ in (*a*) and $\delta = -60°$ in (*b*).

This suggests that the direct convective instability may exist near $\delta = 0°$, but that the shear coupled modes, which tend to have smaller wave-numbers, may exist as the tilt tends towards horizontal. This is suggested also by the energy distributions in table 4. At low angles e_I is small but at large angles there is a large transfer of kinetic energy from the mean to the upslope velocity. In figure 20 (which shows the eigenfunction at a fixed phase) longitudinal vorticity is generated only at the centre of the tank. The thermal excess that exists there for $\delta = -17°$ comes out of the advection of the cross-stream component of the basic stratification. For $\delta = -60°$ the mean temperature gradient $\overline{T}_z$ is nowhere negative, the cross-stream temperature field is everywhere stabilizing. However, at these

angles the effectiveness of the upslope buoyancy is reduced and through the advection term in (6.6) it is possible to have u negative where T is positive. Hence for these large negative angles the shear coupled mode predominates.

One would suspect that at low P_r the shear would be very important and the indirect convective instability with its low wave-numbers would prevail. At high P_r instability would only involve the reverse gradient in $\overline{T}_z$ and would have larger wave-numbers. This is shown in figure 21 which presents results from some calculations for various Prandtl numbers. In air instability occurs at a low Rayleigh number with a long wavelength. At large P_r the instability may approach a condition which is essentially independent of P_r as it would if it became purely convective. Table 5 shows some preliminary data taken from our streak photographs which tends to verify these ideas.

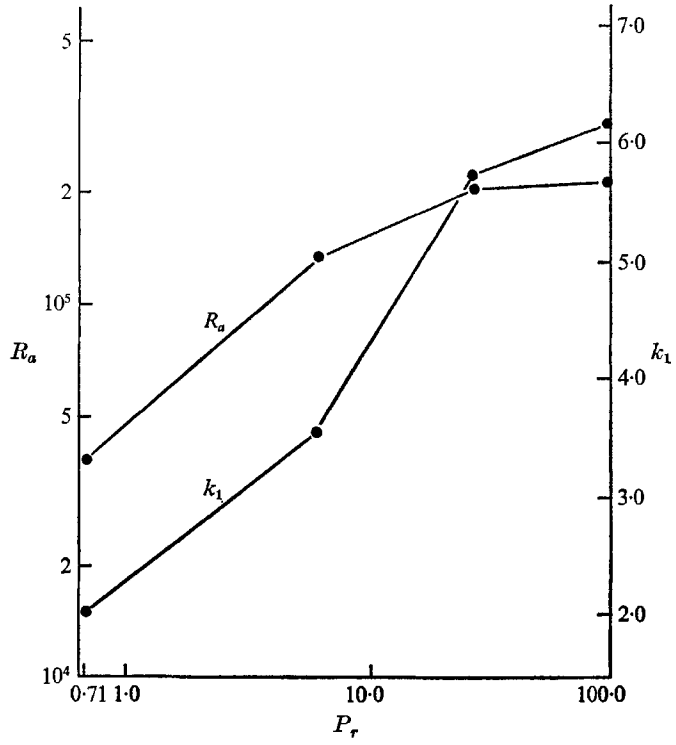

FIGURE 21. Neutral curves for R_a and k_1 as functions of the Prandtl number at $\delta = -45°$.

R_a	δ	P_r	h	e_v	e_u	e_c	e_I
341,000	−17°	6·7	0·04	−1·000	0·958	0·042	−0·001
167,200	−60°	6·7	0·04	−1·000	0·186	0·195	0·623
401,000	−81°	6·7	0·04	−1·000	0·018	0·280	0·701
26,980	−45°	0·71	0·04	−1·000	−0·191	0·009	1·190
135,000	−45°	6·7	0·04	−1·000	0·396	0·136	0·425
$5{\cdot}12 \times 10^6$	−45°	25	0·04	−1·000	0·923	0·100	0·050

TABLE 4. Energy balance for the stationary longitudinal modes

P_r	δ	R_a	k	R_a(theory)	k(theory)
6·7	$-45°$	$1{\cdot}31 \times 10^5$	3·72	$1{\cdot}49 \times 10^5$	3·55
24	$-45°$	$1{\cdot}52 \times 10^5$	5·28	$1{\cdot}92 \times 10^5$	5·61

TABLE 5. Some experimental data for $\delta > 0$

7. Quantitative measurements of the transition points

As the theory was being developed we were trying to make more precise measurements of the events observed in the streak photographs. Of course the glass wall was replaced with the ground aluminium one for this. It was first verified that there were no stationary transverse modes. These were looked for at $\delta = 85°$, $60°$, $30°$, $10°$, $0°$, $-10°$ and $-30°$, by increasing ΔT slowly until the Rayleigh number was above that required for one of the other types of disturbance. We used (i) photographs of streak lines taken looking in along $x = z = 0$, (ii) photographs of longitudinal dye pulses initiated along $y = z = 0$, (iii) temperature profiles taken along $y = z = 0$. In none of these measurements was there any evidence of the stationary transverse modes.

Longitudinal modes were detected by looking for waves in a dye pulse initiated along $x = z = 0$. A run was started by slowly increasing ΔT ($< 0{\cdot}1°/20$ min) and taking photographs every minute from a slightly oblique angle as end-on photography was impossible because of the opacity of the dye. An optical coding arrangement put the applied temperature difference in each picture so that the many hours of data could be scanned through and the onset points determined. Figure 22 (plate 6) shows a typical visualization of onset, along with one end-view streak photograph of the longitudinal rolls which occur for $\delta < 0$.

The travelling modes were detected by looking for oscillations in the thermocouple output of a probe at $x = y = 0$, $z = -0{\cdot}4$. One can alternatively look at dye lines, but because these modes are so weak dye-line observations generally lead to onset parameters three or four times higher than those obtained from the temperature records with a sensitivity of 0·002 °C. The measurements were automated by placing the probe signal on axis Y, and the applied temperature difference ΔT signal on axis X of an X–Y recorder. Before onset a thin slanted line is traced out as each voltage reflects the changing mean conditions. After onset the Y-axis oscillates rapidly and a triangular wedge is formed. The onset is detected as the apex of the wedge. The wavelengths and frequencies of these modes were determined by correlating the signals from two probes displaced in x.

8. Comparison of stability data and theory

The measurements of the instability points are accurate to better than 6 % in R_a and $\pm 0{\cdot}5°$ in δ. However, we must always be prepared to admit that the actual onset points may be below the finite amplitude events which we see, but we hope that our measurements are sufficiently sensitive that we are indeed very near the infinitesimal onset points.

With this in mind we present figures 23–28, which compare the available measurements with the theoretically calculated critical parameters. First of all it should be noted that the theory successfully predicts the absence of any stationary transverse modes for $\delta \lesssim 90°$. Outside of this the agreement is rather good, especially when one considers the complexity of the mean fields. Figures 23 and 24 show the critical Rayleigh numbers for $\delta > 0°$. Figure 25 contains the critical data for $\delta < 0°$. Generally the theory here overestimates the onset of the longitudinal modes, but the shape is reproduced, with cut-offs near the horizontal and vertical positions. Considering that these modes are especially sensitive to the x-dependent part of the temperature field (that part which the mean flow theory fails to reduce to zero at the walls), it would have been somewhat surprising if the agreement were exact.

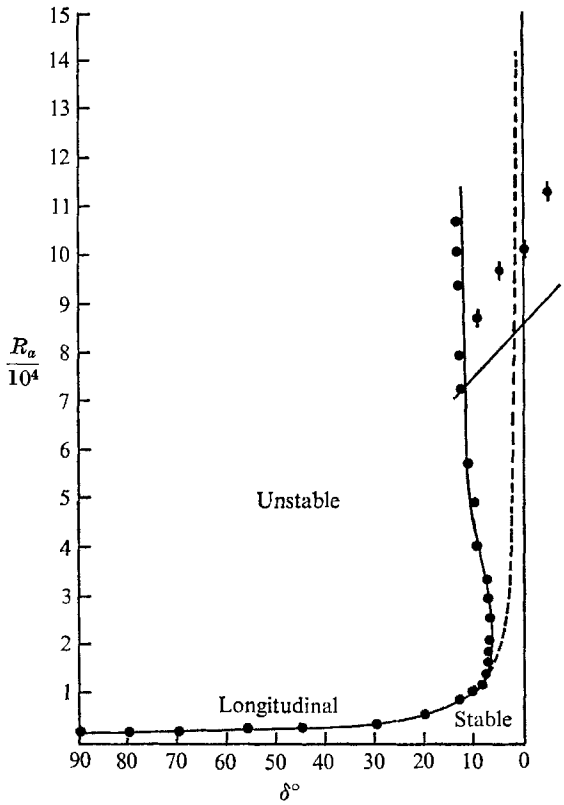

FIGURE 23. Theory (solid) and experimental points for transition to longitudinal (●) and transverse (♦) disturbances for $h = 0{\cdot}027$, $P_r = 6{\cdot}7$. The dashed curve is the theory obtained by assuming the conductive limit throughout.

Figures 26 and 27 contain the wave-number data for the $h = 0{\cdot}04$ longitudinal modes. The error bars here reflect variations in individual roll wavelengths across the tank, which may be due to slight non-linearities or to sidewalls. They give the maximum excursions from the average (represented by the point) of 6 or 7 measurements. The theory predicts wave-numbers which are quite

consistent with the data. The evolution to low wave-numbers as δ tends to $-90°$ indicates strongly the existence of the instability mechanism which allows for coupled convective-shear instabilities in the presence of everywhere positive vertical temperature gradients.

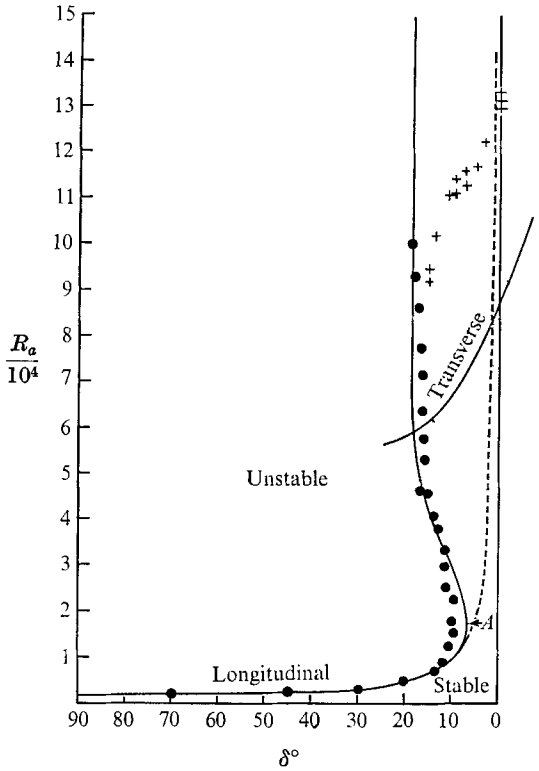

FIGURE 24. Theory and experimental points for transition to longitudinal (●) and to transverse (+) modes for $h = 0{\cdot}04$, $P_r = 6{\cdot}7$.

The theory underestimates the onset of the transverse travelling modes by as much as 80 %. Part of this may be due to the difficulty associated with detecting these very weak fluctuations, but probably some of it is due to the approximate base flow itself since these modes are especially sensitive to the shape of the mean profiles. Also, inherent in both the theory and the technique of measurement was the assumption of a parallel base flow. The real flow is not exactly parallel, and while the longitudinal modes seem to onset uniformly about $x = 0$, the travelling mode transition point seems to depend weakly on x. It is not clear at this time how significant the quasi-parallel assumption is for these modes. The theory again reproduces the general observed features, including the observed frequencies and wave-numbers.

We originally conducted the linear stability analysis in order to understand the physical basis for the rather peculiar behaviour of the experimentally observed instabilities. To this end our effort, especially for the longitudinal modes, was very successful. The chief difficulties in applying this, the usual sort of a stability

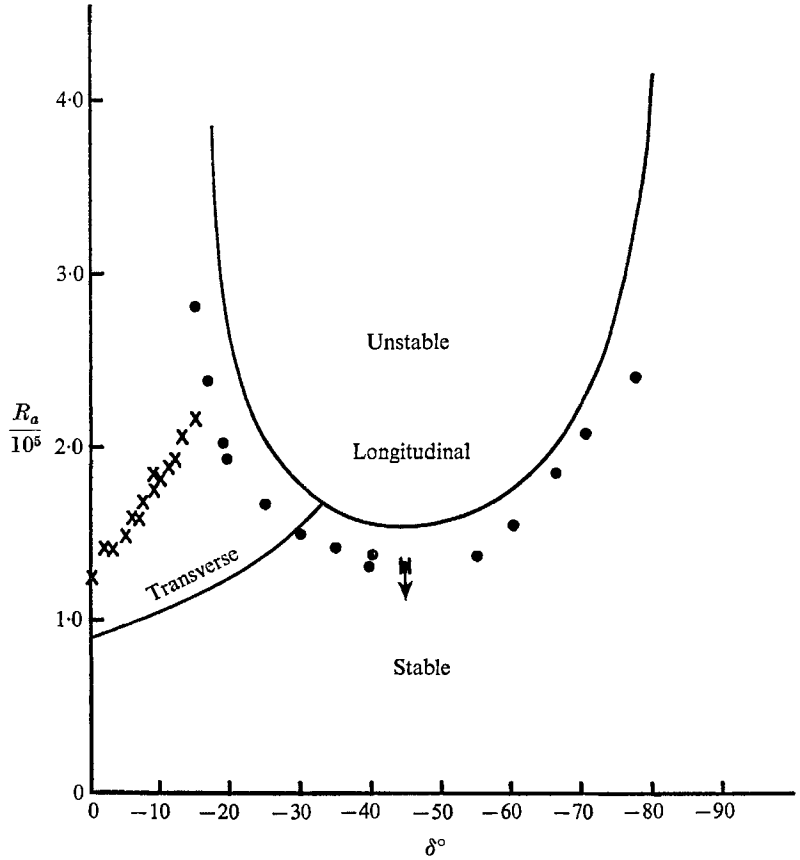

FIGURE 25. Theory and experimental points for transition to longitudinal (●) and to transverse (×) modes for $h = 0{\cdot}04$, $P_r = 6{\cdot}7$, $\delta < 0°$.

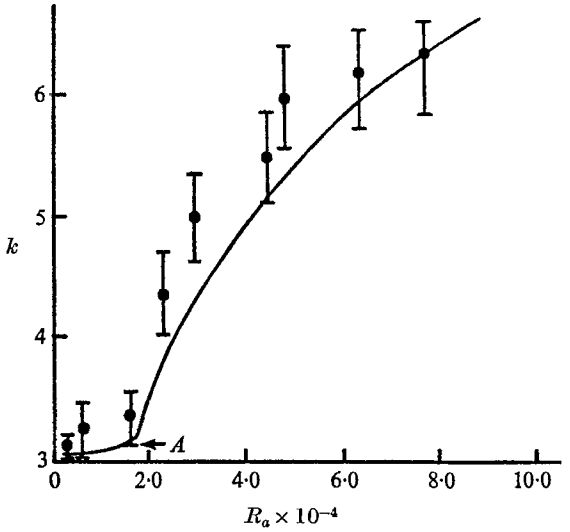

FIGURE 26. Critical wave-numbers for the longitudinal instabilities with $\delta > 0°$, $h = 0{\cdot}04$, $P_r = 6{\cdot}7$. The solid curve is from the theory.

analysis, to the data is that the quasi-parallel assumption, as applied both to the basic flow and to the perturbations, is not completely rigorous. Perhaps higher-order corrections could be added to the present theory but it looks as if this would be a very complicated endeavour. If one wished to pursue the question of these types of instabilities further, it would probably be easier to design an experiment for which the present base flow is exact, namely by constructing a tank with a very small aspect ratio h, with walls maintained at $T_0 = \beta x \mp \frac{1}{2}$.

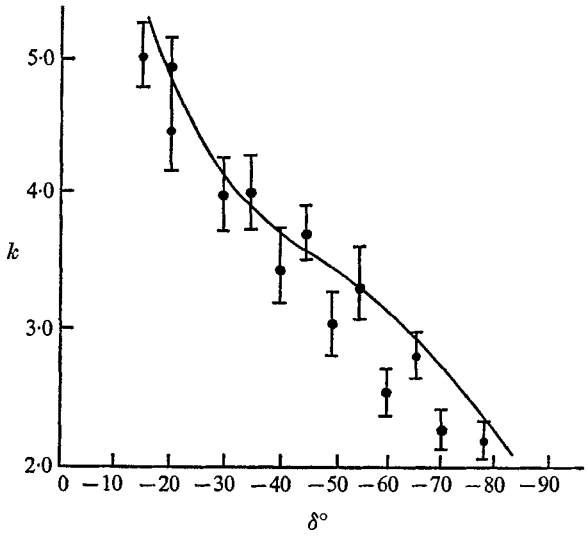

FIGURE 27. Critical wave-numbers for longitudinal instabilities with $\delta < 0°$, $h = 0{\cdot}04$, $P_r = 6{\cdot}7$. The solid curve is from the theory.

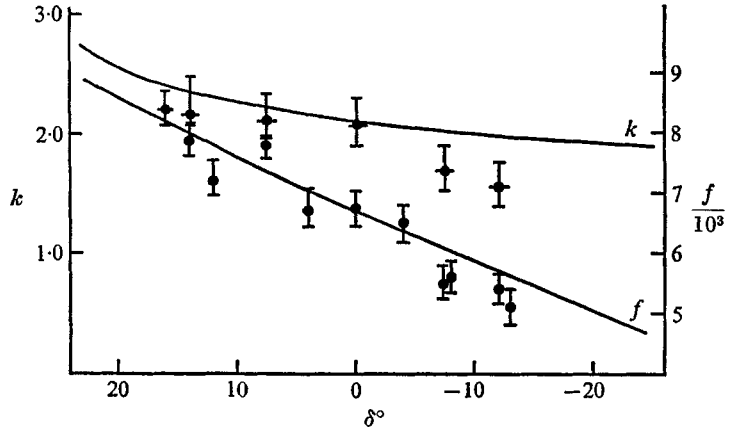

FIGURE 28. Wave-numbers (-●-) and frequencies (●) for the transverse travelling mo des observed at $h = 0{\cdot}04$, $P_r = 6{\cdot}7$. The solid curves are from the theory.

This work was part of a Ph.D. thesis submitted to the M.I.T. Meteorology department. The author would like to thank Prof. E. Mollo-Christensen for his encouragement and helpful suggestions throughout the course of this work. He would also thank Mr Ed Bean, Mr Jimmy Mazzarini and Mr Ken Morey for help

with the technical aspects of the experimental apparatus. Many thanks are also due to N.C.A.R. for making their excellent computing facility available for the production runs. The program testing was done at the M.I.T. computation centre. The work was sponsored by A.F.O.S.R. under contract AF49(638)-1493.

REFERENCES

BAKER, D. J. 1966 *J. Fluid Mech.* **26**, 573.

BATCHELOR, G. K. 1954 *Quart. Appl. Math.* **12**, 209–233.

BIRIKH, R. V., GERSHUNI, G. Z., ZHUKHOVITSKII, E. M. & RUDAKOV, R. N. 1968 *Prikl. Mat. i Mekh.* **32**, 256–263.

BIRIKH, R. V., GERSHUNI, G. Z., ZHUKHOVITSKII, E. M. & RUDAKOV, R. N. 1969 *Prikl. Mat. i Mekh.* **33**, 958.

DAVIS, S. H. 1967 *J. Fluid Mech.* **30**, 465–478.

DEGRAFF, J. G. A. & VAN DER HELD, E. F. M. 1953 *Appl. Sci. Res.* A**3**, 393.

ECKERT, E. R. G. & CARLSON, W. O. 1961 *Int. J. Heat & Mass Transfer*, **2**, 106–120.

ELDER, J. W. 1965*a* *J. Fluid Mech.* **23**, 77–98.

ELDER, J. W. 1965*b* *J. Fluid Mech.* **23**, 99–111.

GALLAGHER, A. & MCD. MERCER, A. 1965 *Proc. Roy. Soc.* A**286**, 117–128.

GERSHUNI, G. Z. & ZHUKHOVITSKII, E. M. 1969 *Prikl. Mat. i Mekh.* **33**, 855.

GILL, A. E. 1966 *J. Fluid Mech.* **26**, 515–536.

GILL, A. E. & DAVEY, A. 1969 *J. Fluid Mech.* **35**, 775–778.

GILL, A. E. & KIRKHAM, C. C. 1970 *J. Fluid Mech.* **42**, 125–127.

HART, J. E. 1971 in preparation.

INGERSOLL, A. P. 1966 *Phys. Fluids* **9**, 682–689.

KOSCHMIEDER, E. 1966 *Beitr. Phys. Atmos.* **39**, 1–11.

KRISHNAMURTI, R. 1970 *J. Fluid Mech.* **42**, 295–321.

KURTWEG, V. H. 1970 *J. Heat Transfer*, **14**, 190.

LIANG, S. F. & ACRIVOS, A. 1970 *Int. J. Heat & Mass Transfer*, **13**, 449.

MIKHLIN, S. G. 1964 *Variational Methods in Mathematical Physics*. New York: Pergammon.

RAYLEIGH, L. 1916 *Phil. Mag.* **32**, series 6.

RUDAKOV, R. N. 1967 *Prikl. Mat. i Mekh.* **31**, 349–355.

SEGEL, L. 1969 *J. Fluid Mech.* **38**, 203–224.

VEST, C. M. & ARPACI, V. S. 1969 *J. Fluid Mech.* **36**, 1.

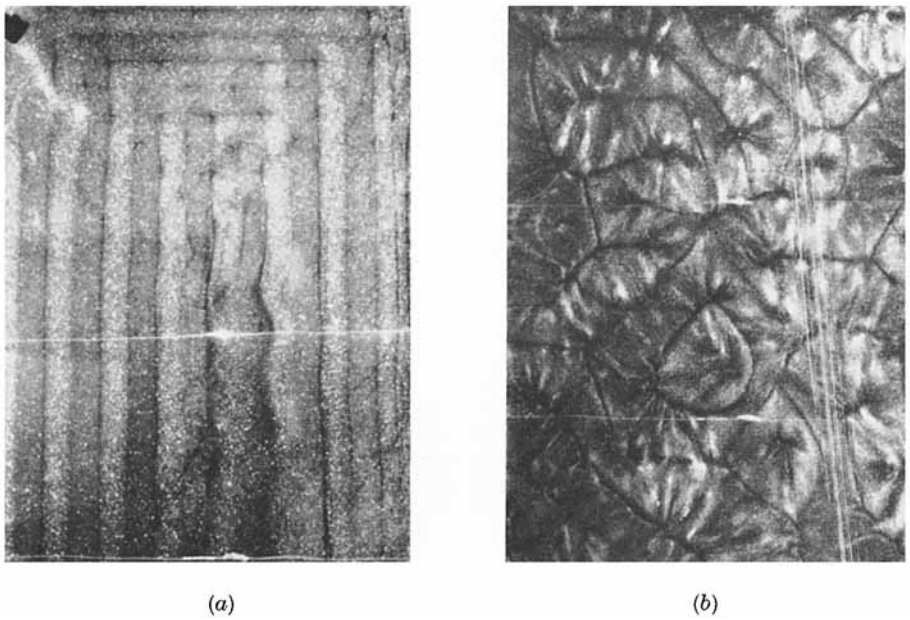

FIGURE 2. Photographs from the visual study with $\delta = 90°$, $h = 0{\cdot}027$.
(*a*) $R_a = 1900$, (*b*) $R_a = 21600$.

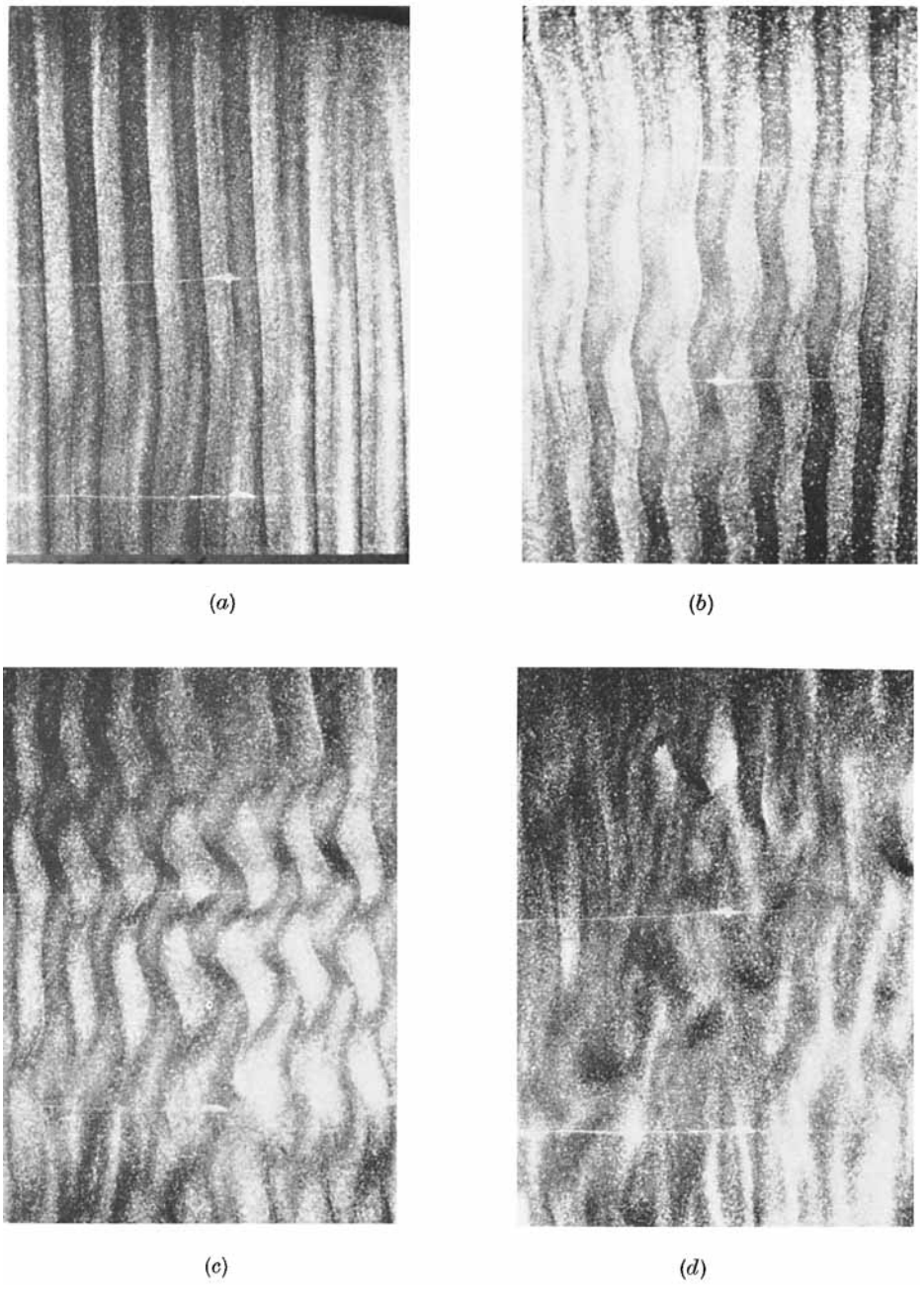

FIGURE 3. Photographs from the visual study with $\delta = 60°$, $h = 0{\cdot}027$.
(*a*) $R_a = 4232$, (*b*) $R_a = 6186$, (*c*) $R_a = 7650$, (*d*) $R_a = 11400$.

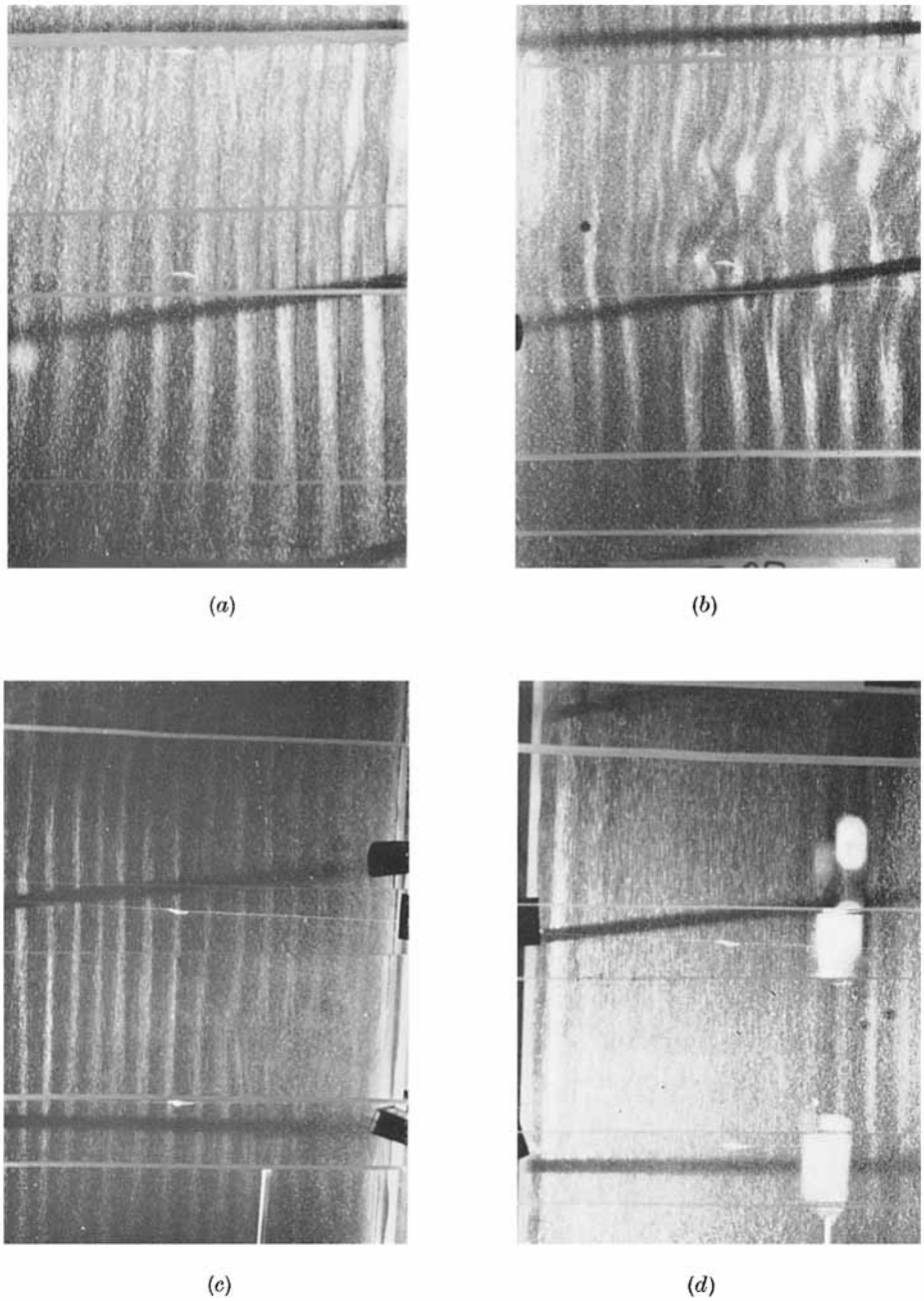

(*a*) (*b*)

(*c*) (*d*)

FIGURE 4. Photographs from the visual study with $\delta = 20°$, $h = 0{\cdot}027$.
(*a*) $R_a = 1{\cdot}17 \times 10^4$, (*b*) $R_a = 2{\cdot}29 \times 10^4$, (*c*) $R_a = 1{\cdot}02 \times 10^5$, (*d*) $R_a = 1{\cdot}22 \times 10^5$.

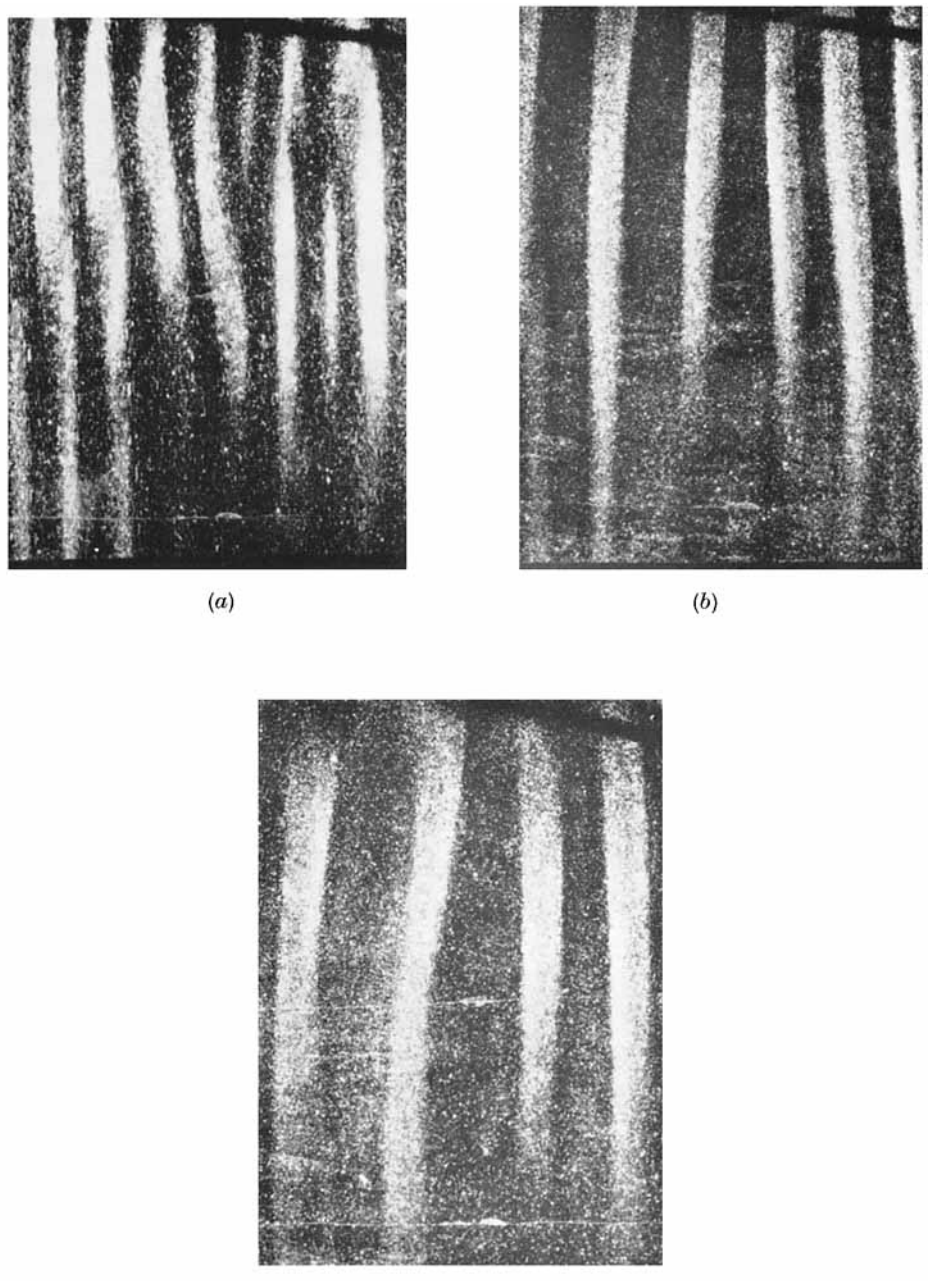

FIGURE 5. Photographs from the visual study with $h = 0{\cdot}04$. (*a*) $R_a = 1{\cdot}84 \times 10^5$, $\delta = -30°$, (*b*) $R_a = 1{\cdot}89 \times 10^5$, $\delta = -60°$, (*c*) $R_a = 3{\cdot}42 \times 10^5$, $\delta = -75°$.

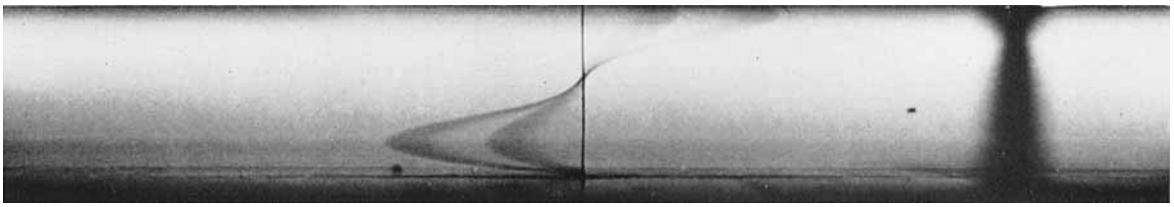

FIGURE 9. Photograph of a dye streak induced along $x = y = 0$ in the unicellular régime with $R_a = 3{\cdot}6 \times 10^4$, $\delta = 0°$, $P_r = 6{\cdot}7$ and $h = 0{\cdot}04$.

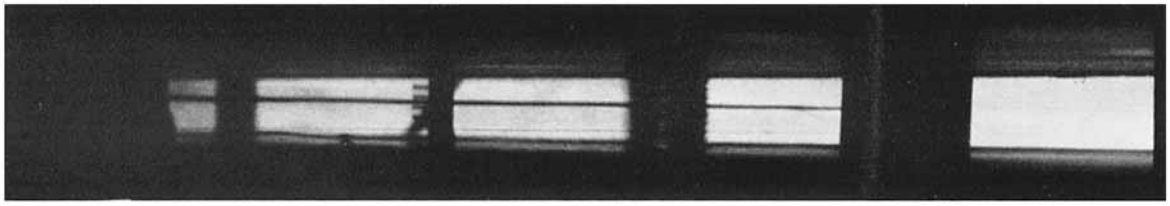

(*a*)

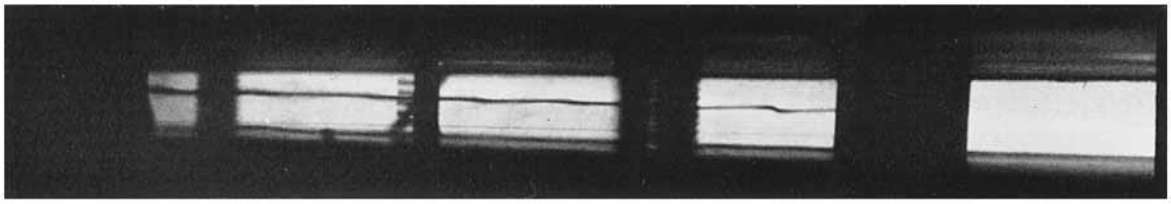

(*b*)

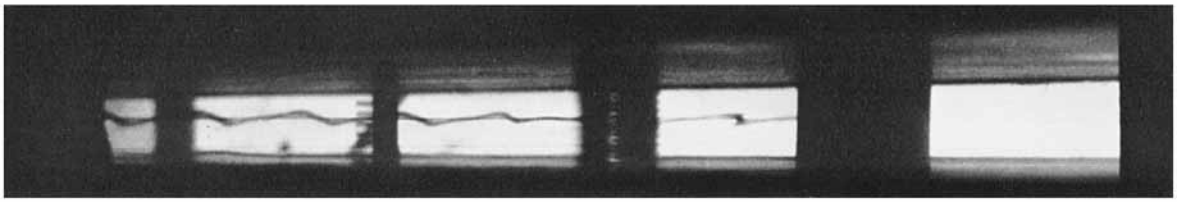

(*c*)

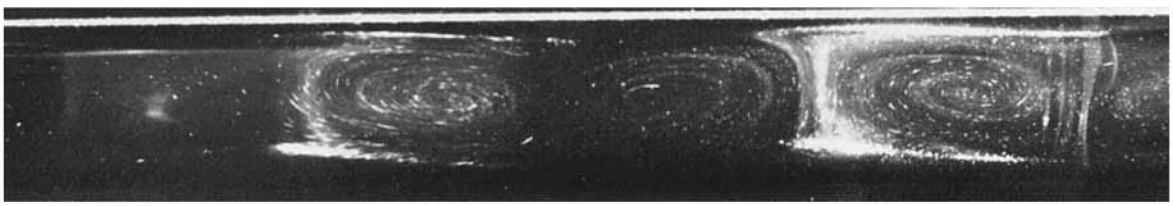

(*d*)

FIGURE 22. Cases (*a*)–(*c*) show the onset of the longitudinal mode at $\delta = 12{\cdot}5°$. The Rayleigh numbers are consequtively 8328, 8854 and 9750. Case (*d*) is an end view streak photographs of the longitudinal rolls at $R_a = 234000$, $\delta = -75°$.